UNIVERSITY OF CALIFORNIA SAN DIEGO

Changes in North Pacific Sea Surface Temperature and Source Water in the California Current Ecosystem

A Thesis submitted in partial satisfaction of the requirements
for the degree Master of Science

in

Oceanography

by

Benjamin Eric Werb

Committee in charge:

Daniel Rudnick, Chair
Mark Merrifield
Brice Semmens
Andrew Thompson

2023

The Thesis of Benjamin Eric Werb is approved, and it is acceptable in quality and form for publication on microfilm and electronically.

University of California San Diego

2023

Dedication

To my parents

Epigraph

“A NOBLE SPIRIT EMBIGGENS THE SMALLEST MAN”

Table of Contents

List of Figures

List of Tables

Acknowledgements

I would first like to acknowledge my advisor, Daniel Rudnick for his incredible support and devotion to my success over the past two years. I have gained so much from our weekly meetings. Thank you for always keeping your door open.

I would also like to acknowledge the community here at Scripps. I have been so fortunate to learn from such great professors, engineers, friends, and colleagues. I have met the greatest people in this past year.

I am most grateful for my family: to my grandparents for loving and caring for me; to my brother, uncles, and aunt for giving me a second home in California; and most of all for my parents, who instilled in me the importance of education and let me find my own path. You have both set the bar far too high.

Chapter 1, in full, is a reprint of the material as it appears in Werb, B.E., & Rudnick, D.L. (2023). Remarkable Changes in the Dominant Modes of North Pacific Sea Surface Temperature. *Geophysical Research Letters*, *50*, e2022GL101078. https://doi. org/10.1029/2022GL101078. The thesis author was the primary investigator and author of this paper.

Vita

2022 Bachelor of Science in Oceanic and Atmospheric Sciences, University of California San Diego

2023 Master of Science in Oceanography, University of California San Diego – Scripps Institution of Oceanography

Publications

Werb, B.E., & Rudnick, D.L. (2023). Remarkable Changes in the Dominant Modes of North Pacific Sea Surface Temperature. *Geophysical Research Letters*, *50*, e2022GL101078. https://doi. org/10.1029/2022GL101078

Field of Study

Oceanography

Abstract of the Thesis

Changes in North Pacific Sea Surface Temperature and Source Water in the California Current Ecosystem

by

Benjamin Eric Werb

Master of Science in Oceanography

University of California San Diego, 2023

Daniel Rudnick, Chair

From 2014 to 2019, there was a period of persistent, record-breaking marine heatwaves in the North Pacific that had significant impacts on the California Current Ecosystem (CCE). This thesis first revisited the calculation of the empirical orthogonal functions (EOFs) and principal components (PCs) of sea surface temperature (SST) in this region. We found that since 2014, there were fundamental changes to the dominant EOFs and PCs. A conclusion was that the Pacific Decadal Oscillation (PDO), a measure of variability in the North Pacific, and other EOF-based metrics may not be as useful as climate continues to change. Next, the thesis provided a first look at the anomaly of dissolved oxygen concentration from the annual cycle as measured

by the California Underwater Glider Network. We gained new insights on the water masses in the CCE and found that a major contributing factor of oxygen anomalies were changes in source water concentration. Finally, the thesis examined the environmental factors influencing ichthyoplankton abundance in the CCE and suggested new indices to reflect the abundances of several prominent northern and southern mesopelagic species.

Introduction

In the last decade there has been unpresented warming in the North Pacific Ocean due to a period of persistent marine heatwaves. The first of which, (popularly) referred to as "The Blob", began offshore of the Gulf of Alaska in early 2014 and caused sea surface temperature (SST) anomalies to peak more than 2.5^{o}C above the mean. This event was further compounded by the onset of the 2014-2016 El Nino and followed by a second powerful marine heatwave in 2019. As a result, there have been broad implications on the California Current Ecosystem, including significant changes to marine habitats and regional weather patterns, but the Pacific Decadal Oscillation (PDO), an important climate index, has not reflected the severity of these changes. Chapter one examines the impact of these marine heatwaves on the dominant spatial modes of North Pacific SST and addresses possible issues in the methods used to compute the PDO Index.

The faults found with basin scale indices such as the PDO highlight the importance of local climate indices that more accurately reflect regional conditions. Furthermore, the advent of autonomous ocean profilers allows for more in depth analysis of specific regions because of an increase in the spatial and temporal resolution of measurements. Chapter two utilizes novel dissolved oxygen data collected by the California Underwater Glider Network (CUGN) to create a climatology of the California Current Ecosystem (CCE) from 2017 – 2023. This high-resolution dissolved oxygen data could help explain important biological processes by improving scientific understanding of the CCE. Therefore, the causes of oxygen anomalies from the annual cycle are of great interest. An overview of the CCE on lines that run offshore of Dana Point, Point Conception, and Monterey Bay, California is provided for dissolved oxygen concentration, salinity, and depth on isopycnal surfaces.

The third chapter delves more into the biological impacts of source water variability in the CCE through analysis of ichthyoplankton abundance in relation environmental factors. For this study we use four decades of data collected by CalCOFI cruises including ichthyoplankton abundance for eight fish species – representing four major habitat categories, temperature, salinity, and dissolved oxygen concentration. The novel approach of this analysis is examining the impact of source water to these species in a specific region rather than across the entire basin.

Chapter 1: Remarkable Changes in the Dominant Modes of North Pacific Sea Surface Temperature

Abstract

The analysis revisits the calculation of the empirical orthogonal functions (EOFs) and principal components (PCs) of sea surface temperature (SST) in the North Pacific from 1950-2021. The first EOF and PC of SST has proven to be such a useful metric of variability in the North Pacific that it is called the Pacific Decadal Oscillation (PDO). We find that the period of persistent marine heatwaves beginning in 2014 caused a fundamental change to the first EOF and PC of SST (calculated using data from 1950-2021) as compared to the established PDO spatial pattern (calculated using data from 1950-1993). The second EOF of SST has also changed during this period, both in spatial pattern and in the amount of variance explained. A conclusion is that the PDO and other EOF based metrics may not be as useful in the future as climate continues to change.

Plain Language Summary

The Pacific Decadal Oscillation (PDO) is a widely used measure of the temperature variability in the North Pacific Ocean. The PDO is the result of a well-known technique called empirical orthogonal function (EOF) analysis that isolates the most energetic modes of variability of the analyzed variable. The first time EOF analysis was applied to oceanographic data was in the 1970's when it was used to identify the most energetic modes of North Pacific sea surface temperature (SST). The first EOF of North Pacific SST has proved so useful as a measure that it received the moniker PDO. Our analysis suggests that a period of persistent marine heatwaves in the North Pacific since 2014 has been so powerful that this first mode of

variability of SST has fundamentally changed and the PDO may not be as useful an indicator as it once was.

Introduction

Sea surface temperature (SST) in the North Pacific has long been known to play a fundamental role in climate variability. Beginning in the 1960s, Jerome Namias noted that patterns of SST anomalies influenced atmospheric variability on large scales (Namias & Cayan, 1981). To identify these patterns, the first empirical orthogonal function (EOF) analyses of North Pacific SST were performed (Davis, 1976; Weare et al., 1976). An EOF analysis in its simplest form takes a variable like SST that is a function of space and time and expresses it as a sum of products of spatial and temporal modes. The spatial modes are typically called EOFs, and the temporal modes are called amplitudes or principal components (PCs). The first EOF and PC proved such a useful measure of large-scale, low-frequency variability in the North Pacific that it was given the name Pacific Decadal Oscillation (PDO) by Mantua et al. (1997). The PDO has proved to be a valuable measure of basin-scale variability in the North Pacific that continues to be used in fisheries (Weber et al., 2021). A number of studies have addressed changes in the PDO temporal index (Bond et al., 2003; Litzow et al., 2020a; Litzow et al., 2020b). The PDO has also been widely used as a metric of climate variability in the North Pacific with effects on atmospheric processes, although, as noted by Newman et al. (2016), this could also be related to the El Niño Southern Oscillation (ENSO).

Since 2014, the eastern North Pacific has experienced a series of marine heatwaves (Bond et al., 2015) with pronounced effects on the California Current System (Zaba & Rudnick, 2016). We address the question of how this period of anomalous warmth in the eastern North Pacific is reflected in the EOFs of North Pacific SST. To ensure that recent warming contributes

to the variability we do not remove a trend before applying the EOF analysis. Retaining the trend is consistent with the original EOF analysis of the North Pacific (Davis, 1976) and more recently by Johnstone and Mantua (2014) who calculated the EOFs of SST east of the dateline. Notably, Johnstone and Mantua (2014) define a Northeast Pacific (NEP) index by averaging over the positive region of their first EOF in the eastern Pacific. At issue is whether the EOFs describe variability relative to the trend, or whether they are influenced by warming at the end of the record. By calculating EOFs and PCs over records of increasing length, we demonstrate that this period of persistent marine heatwaves (MHWs) has transformed the spatial pattern of the first EOF of North Pacific SST to such an extent that the PDO may no longer be as serviceable a metric of SST variability as currently regarded.

Data

We use monthly mean SST for the period 1950-2021 in the region 120°E-110°W, 20°N-60°N, from the NOAA Extended Reconstructed Sea Surface Temperature V5 data product (ERSSTv5) with 2° resolution in longitude and latitude and confirm our results with the HadISST data product (see supplementary material). ERSSTv5 consists of in situ measurements collected from ships, buoys, and Argo floats, excluding remotely sensed satellite data, and uses a series of reconstruction techniques to extend global records back to 1854 (Huang et al., 2017b). Spatial coverage is the foundation of a strong EOF/PC analysis (Huang et al., 2017b) so this study uses only the data from the modern era, following previous studies (Newman et al., 2003). ERSSTv5 and HadISST are both data products derived from observations and there are systematic SST differences between the two products in the central and north-eastern Pacific causing large discrepancies in the resulting PDO indices (Wen et al., 2014). We use the ERSSTv5 product, following the NOAA PDO calculation.

Analysis

The objective of this analysis is to revisit the calculation of EOFs and PCs as first done by Davis (1976). The first step is to remove the seasonal cycle from ERSSTv5 by computing the average monthly temperature and subtracting it from each respective month. The result of this procedure is a data set of SST anomalies (SSTa) relative to the annual cycle. The global warming trend was not removed from the time series so that the trend contributes to the variance described by the EOFs; previously Johnstone and Mantua (2014) also did not remove a trend for the same reason. We apply an EOF analysis to find the most energetic modes of variance. The resulting EOFs and PCs are orthogonal to one another and are ordered by the variance explained. The first five EOFs account for over 50% of the total variance, the detailed distribution between the EOFs is covered below. To calculate the EOFs and PCs, we use a singular value decomposition of the anomaly data set.

The PDO spatial pattern and Index were recreated with SSTa from ERSSTv5 (Mantua et al., 1997) by doing the EOF analysis only for data during 1950-1993. The EOF from this analysis is then projected onto the full time series to create the PDO Index and normalized to have unit length in the L2 norm.

The EOF analysis was done on successively longer time series starting with 1950-1970 and increasing yearly to 1950-2021. The results of this analysis are shown in several ways including EOF/PC pairs and by variance explained. Percent variance is calculated by squaring the singular values and dividing by the trace of the matrix squared. As a measure of structure, we calculate the percentage of the grid points where the EOFs are greater than zero and find that the structure of the EOFs change over time. See supplementary material 4 for a bootstrap calculation assessing significance.

Results

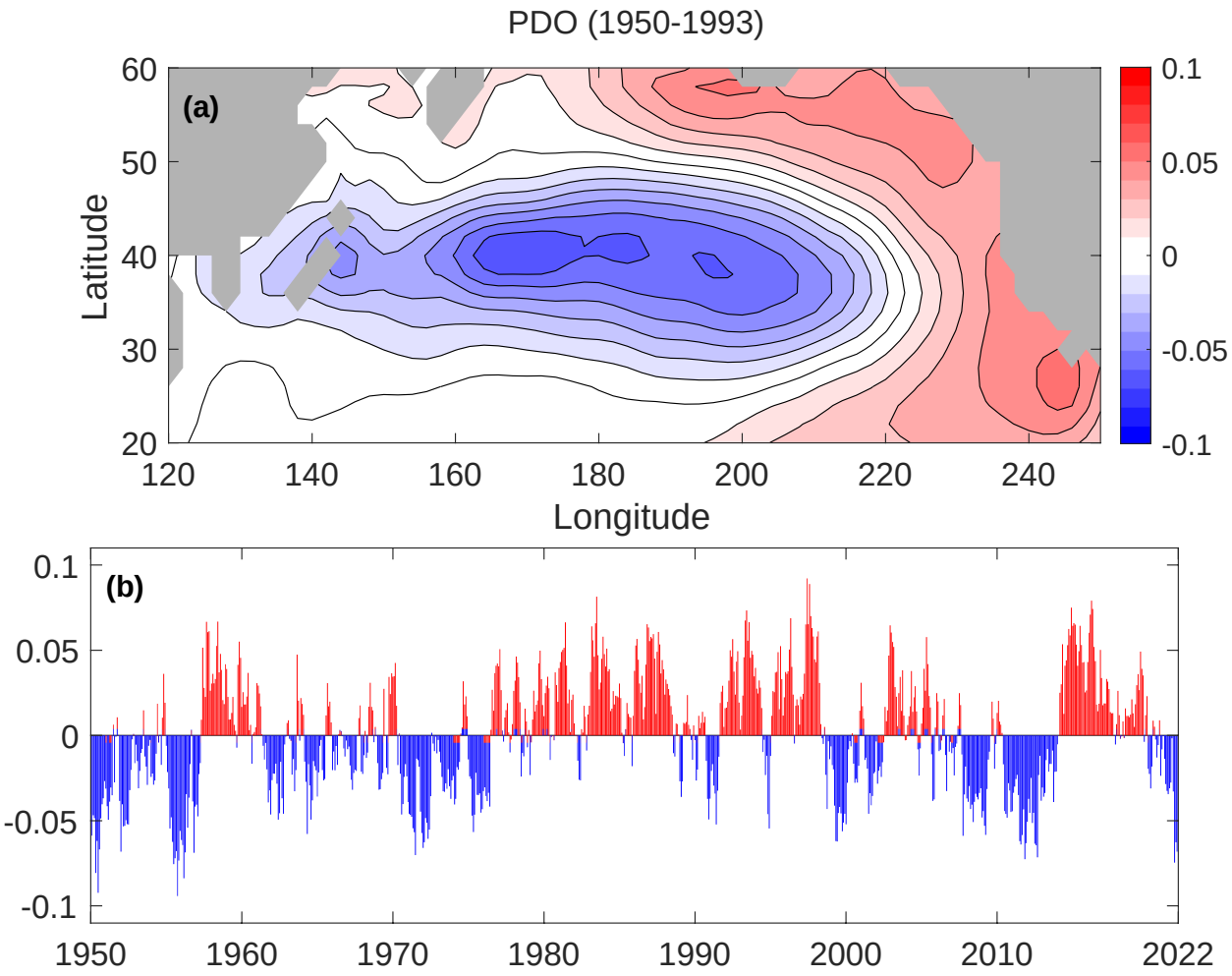

Figure 1.1 (a) PDO spatial pattern calculated as the first EOF of SST from 1950-1993. (b) The PDO Index formed by the projection of the PDO spatial pattern onto the full time series of SST anomalies from 1950-2021.

The spatial pattern of the PDO for this paper is calculated as the first EOF of SST from 1950-1993, exclusively removing the annual cycle, and the projection onto this spatial pattern produces the PDO index (Figure 1.1). This is distinct from the original calculation which is done on data detrended using the anomaly deviation method (Mantua et al., 1997; Zhang et al., 1997). The correlation coefficient between our version of the PDO and the original PDO is 0.97. That the correlation is so high suggests that our data and procedure are close enough to those used

originally, and that whether a trend is removed from the data has little effect on the result. The important point here is that the PDO spatial pattern is fixed in 1993 while the PDO Index evolves.

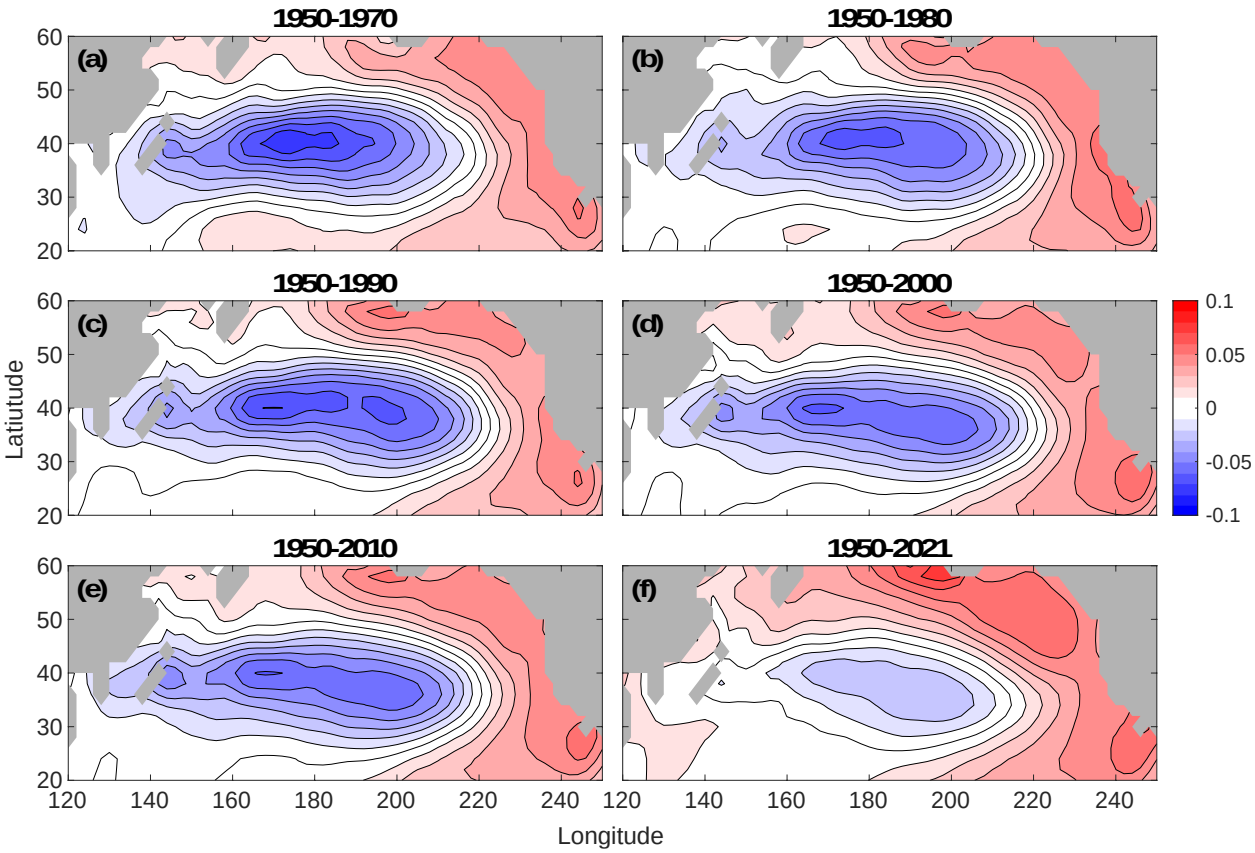

Figure 1.2 The first EOF of SST over the PDO region (120°E-110°W 20°N-60°N). (a)-(f) show the same spatial pattern calculation with a changing time series highlighting the effects of ocean warming in the last decade.

The first EOF of SST is calculated in blocks starting with the period 1950-1970 and increasing by 10-year increments to a maximum of 1950-2021 (Figure 1.2). The spatial pattern of the first EOF is relatively consistent for successively longer time periods up to 1950-2010 (Figure 1.2a-e). The addition of the last decade to the calculation results in a significant change in the EOF, with a larger positive region in the eastern Pacific and a smaller negative lobe in the central Pacific. This change is due to persistent and strongly positive SST anomalies in the

eastern and interior/western North Pacific. At its peak, the first MHW in this period (popularly referred to as "The Blob"; Bond et al., 2015) reached a temperature anomaly of +2.5°C, and impacted both marine ecosystems and weather patterns. This was followed by the 2014-2016 El Niño (L'Heureux et al., 2017; Rudnick et al., 2017), and the 2019 MHW (Amaya et al., 2020), resulting in continued warm anomalies in the eastern North Pacific. This anomalous warmth has largely remained in the California Current System (Ren & Rudnick, 2021b), resulting in a fundamental change to the leading EOF of SST in the North Pacific.

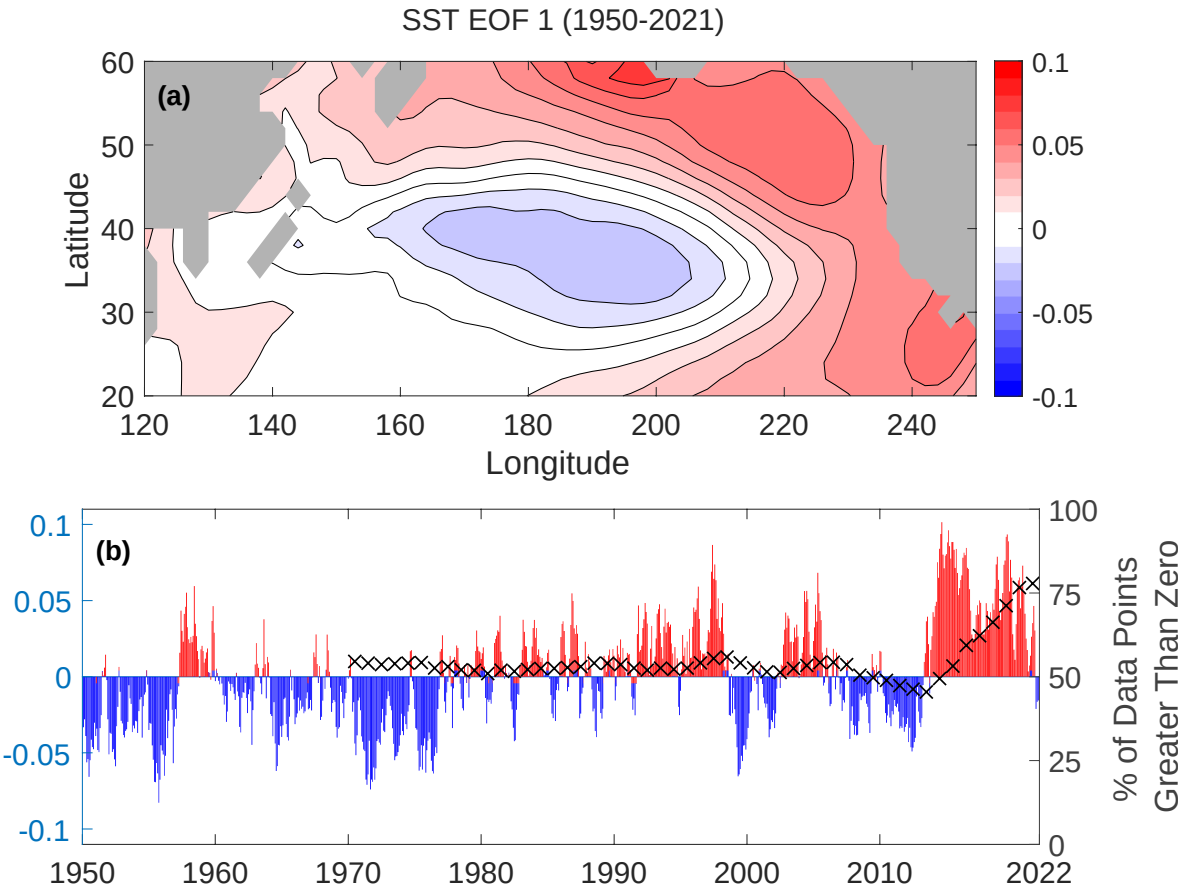

Figure 1.3 (a) The first EOF of SST over the PDO region for the entire time series (1950-2021). **(b)** The principal component for the first EOF is depicted on the left y-axis, with red bars indicating positive years and blue bars indicating negative years. The right y-axis (x symbols) depicts the percentage of grid points greater than zero in the first EOF from 1970-2021.

The first PC for the period 1950-2021 is dominated by an era of frequent MHW's from 2014-2021 (Figure 1.3). The combination of this strong warming phase at the end of the record and the cold phase at the beginning in this PC reflects a warming trend during 1950-2021 in the eastern Pacific. The inclusion of the trend in the time series allows it to be represented in the first PC and shows that a great deal of the warming is in recent years. This PC (Figure 1.3b) should be compared to the PDO Index (Figure 1.1b), especially regarding the recent warming. The PDO Index became negative in 2019 due to the impacts of persistently positive SSTa in the interior north Pacific on the negative lobe of its spatial pattern, while the first PC of the complete record remained positive until very late in 2021. That is, the first PC of the full time series fairly reflected the recent warming in the eastern Pacific while the PDO Index did not.

A measure of the spatial shape of the first EOF is the number of positive values in the 2° by 2° spatial grid. The first EOF is calculated over successively longer time periods, increasing by one year each, and the percentage of positive values is plotted in Figure 1.3b. The size of the positive region in the eastern Pacific stays relatively constant with roughly half the points greater than zero until 2014, after which the positive region rapidly increases in size to cover 77% of the North Pacific in 2021. The results are similar for HadISST data, with the positive region covering 65% of the Pacific (S1-3). Such a fast rate of change in the shape of the first EOF is unprecedented, with roughly one-quarter of the North Pacific's area between 20-60°N changing polarity in the EOF. The relative consistency in the spatial pattern before 2014 is strong support for the usefulness of the PDO during the period 1950-2014 while the changes since 2014 suggest that the PDO is no longer the best descriptor of variance in SST in the north Pacific.

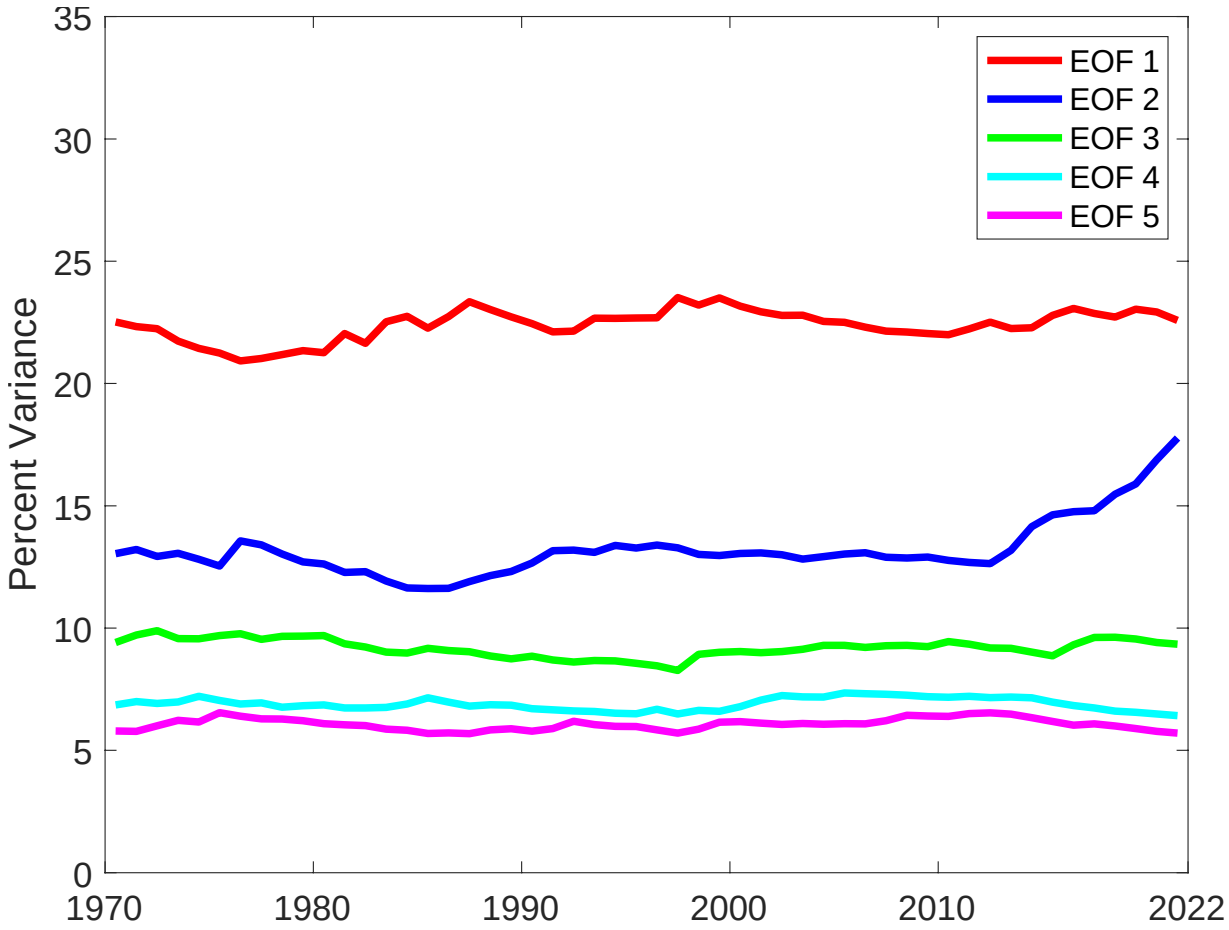

Figure 1.4 The percent variance accounted for by each EOF of the SST data set over the period of 1970-2021.

The percent variance explained by each of the first 5 EOFs is calculated from successively longer time periods (Figure 1.4). Throughout the record, EOF 1 has explained approximately 23% of the variance in SST. EOF 2 accounted for approximately 13% of the variance in SST until 2014, after which it increased to nearly 18%. This increase occurred simultaneously with the changing spatial pattern of EOF 1 in response to the MHW's. Interestingly the MHW's have changed patterns in such a fundamental way that the second EOF has risen in importance for describing SST variability in the North Pacific.

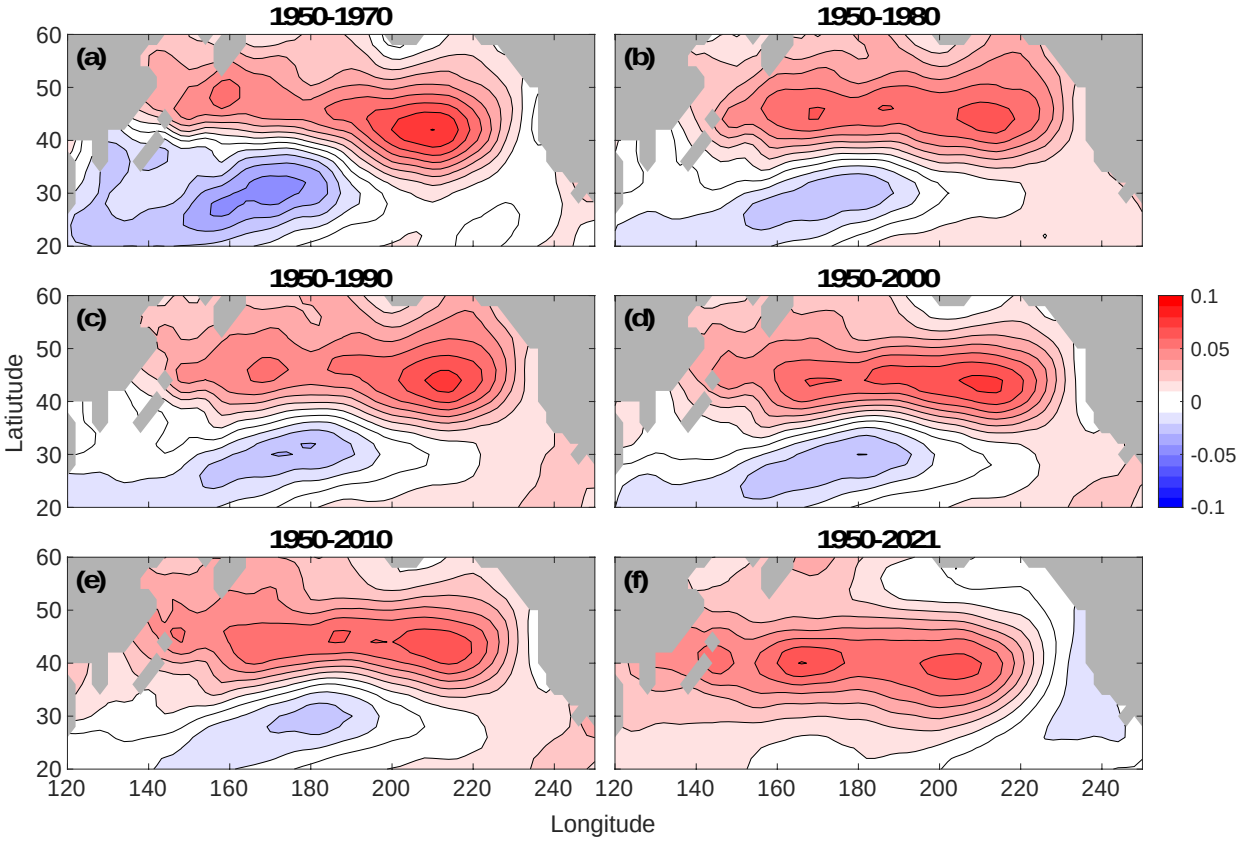

Figure 1.5 The second EOF of SST over the PDO region (120°E-110°W 20°N-60°N). (a)-(f) show the same spatial pattern calculation with a changing time series.

At the start of the time series the second EOF of SST was composed of two distinct lobes: positive in the north and negative in the south (Figure 1.5). Like EOF 1, this pattern remains consistent through 2010 (a-e), and then undergoes a change of shape after adding the most recent decade to the record (f). The positive lobe has recently filled up nearly all the North Pacific (Figure 1.5f). With the growth of this positive lobe, a small negative lobe has grown in the eastern North Pacific. In a sense, there has been a reshuffling of the regions affected by EOFs 1 and 2 (comparing Figures 1.2 and 1.5) in response to the period of persistent MHW's from 2014-2021. There is no longer a single EOF/PC pair that describes variance in the 30-50°N latitude band where the first two EOFs are both large.

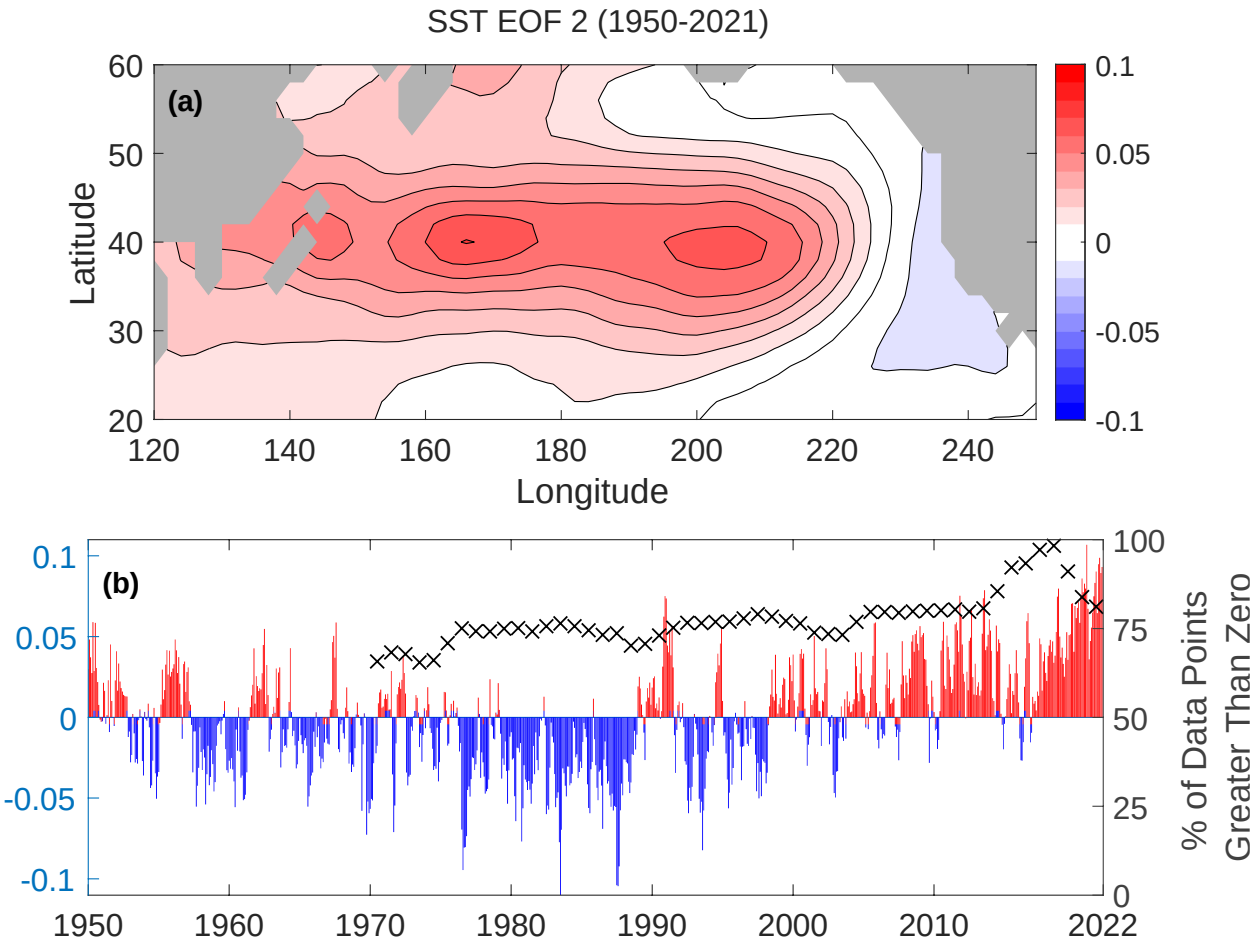

Figure 1.6 (a) The second EOF of SST over the PDO region for the entire time series (1950-2021). (b) The principal component for the second EOF is depicted on the left y-axis using colored bars. The right y-axis (x symbols) depicts the percentage of data points greater than zero in the second EOF from 1970-2021.

The second PC is mostly positive from 1990-2021 and strongly positive from 2014-2021 (Figure 1.6b), reflecting the positive SSTa across much of the North Pacific that EOF 1 alone does not capture. The weak negative lobe in the second EOF lessens the warming near the coast of North America. As EOF 2 describes less of the variance than EOF 1, it might be expected that its shape is more variable when calculated over different time periods, interestingly, the positive lobe in EOF 2 has grown steadily when calculated over successively longer time periods (Figure 1.6b, x-ticks). The positive lobe of EOF 2 filled up 98% of the North Pacific when calculated over the period 1950-2018 and similarly for HadISST data at 93% (S1-6). While EOF 2 has not

been invoked as often as the PDO as a measure of SST variability, the robust evolution since 2014 is still worthy of note.

Conclusions

The fundamental result of this study is that the first EOF of SST in the North Pacific has changed starting in 2014. For more than twenty years, the PDO has been used to describe the state of the Pacific Ocean. However, since the marine heatwave of 2014, there have been remarkable changes to the dominant mode of SST in the North Pacific. The spatial pattern of the first EOF of SST from 1950-2021 is notably different from the PDO, suggesting that though the PDO served as a useful metric of SST variations until 2014 (Johnstone & Mantua, 2014), it may no longer be as effective a climate index for the Pacific Ocean. From 1950 until the 2014 MHW, the first EOF remained consistent in its proportion of positive and negative regions with both taking up roughly half the area of the North Pacific (and with the positive region taken to be the eastern Pacific). When EOFs are calculated from 1950 to endpoints after 2014, the first EOF has a maximum positive region covering 77% of the North Pacific, with a PC indicating the largest anomalies on record. These changes to the first EOF/PC of North Pacific SST are nothing short of remarkable.

In concert with these changes, the second EOF/PC of SST has also undergone profound evolution since 2014. This second EOF now accounts for approximately 18% of the variability growing from 13% during the 1950-2013 period. The spatial structure of the second EOF now is positive over almost the entire basin, with a PC that has grown strongly positive in the last several years. Thus, the second EOF/PC describes warming over much of the Pacific not in the positive lobe of the first EOF.

A relevant aspect of our analysis is that we did not remove a trend from the data before calculating the EOFs and PCs. This is consistent with the original calculations of EOFs in the North Pacific (Davis, 1976) and more recent analysis by Johnstone and Mantua (2014), but inconsistent with the definition of the PDO which did have a global mean trend removed (Mantua et al., 1997; Zhang et al., 1997). Whether or not a trend was removed had little effect on the first EOF, and thus the PDO, until 2014. Two of our results lead to this conclusion: first, our first PC calculated between 1950-1993 agreed with the PDO with a correlation coefficient of 0.97; and second, our first EOF calculated with successively longer time series did not change in shape until 2014. There are many approaches to removing a trend from time series (Deser & Phillips, 2021; Frankignoul et al., 2017; Solomon & Newman, 2012). We investigated two of these approaches: first we removed a least-squares fit of a line to the global average temperature as in the original definition of the PDO (S2), and second, we removed a least-squares fit of a line from each grid point in the North Pacific (S3). In each case the EOF analysis reproduced the PDO spatial pattern and index, suggesting that the PDO remains a good measure for the variability relative to the trend. In general, removal of a trend (as by least-squares fitting of a line, for example) tends to deemphasize the ends of a record. In our analysis, the inclusion of the trend highlights the fact that the warming in the eastern Pacific has increased notably in recent years, a fact that would be obscured if a linear trend had been removed.

The PDO is recognized to be a result of many processes that may cause temperature variability (Newman et al., 2016) rather than any singular phenomenon. The many processes that affect SST have apparently combined to create both this era of frequent marine heatwaves beginning in 2014 and a fundamental change to the first mode of SST. The persistence of the marine heatwaves was studied by Di Lorenzo and Mantua (2016) who also invoked a number of

interacting processes, suggesting that the variance described by the PDO would increase in a warmer climate. Di Lorenzo and Mantua (2016) explicitly removed a trend before calculating the EOFs of SST, so that their EOFs described variance relative to the trend. The PDO is based on a constant spatial pattern defined by the EOF that described the most variance of SST through the mid 1990's. However, there is no guarantee that the EOFs of SST will remain constant as climate change continues. This concern about indices based on EOFs applies also to the North Pacific Gyre Oscillation (Di Lorenzo et al., 2008), which describes variance in sea surface height.

The PDO is widely used as a measure of temperature in the eastern boundary upwelling system along the west coast of North America (for example, Weber et al., 2021). The period of persistent marine heatwaves since 2014 has made the PDO less useful as an index of temperature in this region because it does not reflect the recent increase. In general, using PCs from a basin-wide analysis as indices of temperature for specific regions may be problematic because the influences from distant parts of the basin affect the PCs. Options moving forward may include: (1) updating the definition of the first mode of temperature variability, as we have done here, (2) explicitly accounting for the trend in addition to the PDO for a measure of temperature, or (3) defining a new temperature metric in a specified area in the region as is done for the various measures of El Niño (Trenberth, 1997) or more recently as in the NEP index (Johnstone & Mantua, 2014). Interestingly, the NEP was first published just before the recent period of MHWs, and the value of the approach championed in Johnstone and Mantua (2014) has only increased. The wide-ranging effects of the recent period of MHWs are likely to be seen in continuing studies of the eastern North Pacific.

Acknowledgments

We gratefully acknowledge the support of the National Oceanic and Atmospheric Administration through the Global Ocean Monitoring and Observing program (NA20OAR4320278) and the Southern California Coastal Ocean Observing System (NA21NOS0120088). We thank Nate Mantua and an anonymous reviewer for helpful comments.

Open Research

We use monthly mean SST for the period 1950-2021 in the region 120°E-110°W, 20°N-60°N, from the NOAA Extended Reconstructed Sea Surface Temperature V5 data set (Huang et al., 2017a), retrieved from https://psl.noaa.gov/data/gridded/data.noaa.ersst.v5.html on January 12, 2022. The Pacific Decadal Oscillation Index was downloaded from https://www.ncei.noaa.gov/access/monitoring/pdo/ on October 21, 2022.

Chapter 1, in full, is a reprint of the material as it appears in Werb, B.E., & Rudnick, D.L. (2023). Remarkable Changes in the Dominant Modes of North Pacific Sea Surface Temperature. *Geophysical Research Letters*, *50,* e2022GL101078. https://doi. org/10.1029/2022GL101078. The thesis author was the primary investigator and author of this paper.

References

Amaya, D. J., Miller, A. J., Xie, S. P., & Kosaka, Y. (2020). Physical drivers of the summer 2019 North Pacific marine heatwave. *Nature Communications, 11*(1). doi:10.1038/s41467-020-15820-w

Bond, N. A., Cronin, M. F., Freeland, H., & Mantua, N. (2015). Causes and impacts of the 2014 warm anomaly in the NE Pacific. *Geophysical Research Letters, 42*(9), 3414-3420. doi:10.1002/2015gl063306

Bond, N. A., Overland, J. E., Spillane, M., & Stabeno, P. (2003). Recent shifts in the state of the North Pacific. *Geophysical Research Letters, 30*(23). doi:10.1029/2003gl018597

Davis, R. E. (1976). Predictability of sea surface temperature and sea level pressure anomalies over the North Pacific Ocean. *J. Phys. Oceanogr., 6*(3), 249-266.

Deser, C., & Phillips, A. S. (2021). Defining the Internal Component of Atlantic Multidecadal Variability in a Changing Climate. *Geophysical Research Letters, 48*(22). doi:10.1029/2021GL095023

Deser, C., Simpson, I. R., McKinnon, K. A., & Phillips, A. S. (2017). The Northern Hemisphere Extratropical Atmospheric Circulation Response to ENSO: How Well Do We Know It and How Do We Evaluate Models Accordingly? *Journal of Climate, 30*(13), 5059-5082. doi:10.1175/Jcli-D-16-0844.1

Deser, C., Simpson, I. R., Phillips, A. S., & McKinnon, K. A. (2018). How Well Do We Know ENSO's Climate Impacts over North America, and How Do We Evaluate Models Accordingly? *Journal of Climate, 31*(13), 4991-5014. doi:10.1175/Jcli-D-17-0783.1

Di Lorenzo, E., & Mantua, N. (2016). Multi-year persistence of the 2014/15 North Pacific marine heatwave. *Nature Clim. Change, advance online publication*. doi:10.1038/nclimate3082

Di Lorenzo, E., Schneider, N., Cobb, K. M., Franks, P. J. S., Chhak, K., Miller, A. J., McWilliams, J. C., Bograd, S. J., Arango, H., Curchitser, E., Powell, T. M., & Riviere, P. (2008). North Pacific Gyre Oscillation links ocean climate and ecosystem change. *Geophysical Research Letters, 35*(8). doi:10.1029/2007gl032838

Frankignoul, C., Gastineau, G., & Kwon, Y. O. (2017). Estimation of the SST Response to Anthropogenic and External Forcing and Its Impact on the Atlantic Multidecadal Oscillation and the Pacific Decadal Oscillation. *Journal of Climate, 30*(24), 9871-9895. doi:10.1175/Jcli-D-17-0009.1

Huang, B., Thorne, P. W., Banzon, V. F., Boyer, T., Chepurin, G., Lawrimore, J., Menne, M. J., Smith, T. M., Vose, R. S., & Zhang, H.-M. (2017a). NOAA Extended Reconstructed Sea Surface Temperature (ERSST), Version 5, doi: 10.7289/V5T72FNM. Retrieved January 2022, from NOAA National Centers for Environmental Information

Huang, B. Y., Thorne, P. W., Banzon, V. F., Boyer, T., Chepurin, G., Lawrimore, J. H., Menne, M. J., Smith, T. M., Vose, R. S., & Zhang, H. M. (2017b). Extended Reconstructed Sea Surface Temperature, Version 5 (ERSSTv5): Upgrades, Validations, and Intercomparisons. *Journal of Climate, 30*(20), 8179-8205. doi:10.1175/Jcli-D-16-0836.1

Johnstone, J. A., & Mantua, N. J. (2014). Atmospheric controls on northeast Pacific temperature variability and change, 1900-2012. *Proceedings of the National Academy of Sciences of the United States of America, 111*(40), 14360-14365. doi:10.1073/pnas.1318371111

L'Heureux, M. L., Takahashi, K., Watkins, A. B., Barnston, A. G., Becker, E. J., Di Liberto, T. E., Gamble, F., Gottschalck, J., Halpert, M. S., Huang, B. Y., Mosquera-Vasquez, K., & Wittenberg, A. T. (2017). Observing and Predicting the 2015/16 El Nino. *Bulletin of the American Meteorological Society, 98*(7), 1363-1382. doi:10.1175/Bams-D-16-0009.1

Litzow, M. A., Hunsicker, M. E., Bond, N. A., Burke, B. J., Cunningham, C. J., Gosselin, J. L., Norton, E. L., Ward, E. J., & Zador, S. G. (2020a). The changing physical and ecological meanings of North Pacific Ocean climate indices. *Proceedings of the National Academy of Sciences of the United States of America, 117*(14), 7665-7671. doi:10.1073/pnas.1921266117

Litzow, M. A., Malick, M. J., Bond, N. A., Cunningham, C. J., Gosselin, J. L., & Ward, E. J. (2020b). Quantifying a Novel Climate Through Changes in PDO-Climate and PDO-Salmon Relationships. *Geophysical Research Letters, 47*(16). doi:10.1029/2020GL087972

Mantua, N. J., Hare, S. R., Zhang, Y., Wallace, J. M., & Francis, R. C. (1997). A Pacific interdecadal climate oscillation with impacts on salmon production. *Bulletin of the American Meteorological Society, 78*(6), 1069-1079.

Namias, J., & Cayan, D. R. (1981). Large-scale air-sea interactions and short-period climatic fluctuations. *Science, 214*, 869-876.

Newman, M., Alexander, M. A., Ault, T. R., Cobb, K. M., Deser, C., Di Lorenzo, E., Mantua, N. J., Miller, A. J., Minobe, S., Nakamura, H., Schneider, N., Vimont, D. J., Phillips, A. S., Scott, J. D., & Smith, C. A. (2016). The Pacific Decadal Oscillation, Revisited. *Journal of Climate, 29*(12), 4399-4427. doi:10.1175/Jcli-D-15-0508.1

Newman, M., Compo, G. P., & Alexander, M. A. (2003). ENSO-forced variability of the Pacific decadal oscillation. *Journal of Climate, 16*(23), 3853-3857. doi:Doi 10.1175/1520-0442(2003)016<3853:Evotpd>2.0.Co;2

Rayner, N. A., Parker, D. E., Horton, E. B., Folland, C. K., Alexander, L. V., Rowell, D. P., Kent, E. C., & Kaplan, A. (2003). Global analyses of sea surface temperature, sea ice, and night marine air temperature since the late nineteenth century. *Journal of Geophysical Research-Atmospheres, 108*(D14). doi:10.1029/2002jd002670

Ren, A. S., & Rudnick, D. L. (2021). Temperature and salinity extremes from 2014-2019 in the California Current System and its source waters. *Communications Earth & Environment, 2*. doi:10.1038/s43247-021-00131-9

Rudnick, D. L., Zaba, K. D., Todd, R. E., & Davis, R. E. (2017). A climatology of the California Current System from a network of underwater gliders. *Progress in Oceanography, 154*, 64-106. doi:10.1016/j.pocean.2017.03.002

Solomon, A., & Newman, M. (2012). Reconciling disparate twentieth-century Indo-Pacific ocean temperature trends in the instrumental record. *Nature Climate Change, 2*(9), 691-699. doi:10.1038/Nclimate1591

Trenberth, K. E. (1997). The definition of El Nino. *Bulletin of the American Meteorological Society, 78*(12), 2771-2777. doi:10.1175/1520-0477(1997)078<2771:Tdoeno>2.0.Co;2

Weare, B. C., Navato, A. R., & Newell, R. E. (1976). Empirical Orthogonal Analysis of Pacific Sea-Surface Temperatures. *Journal of Physical Oceanography, 6*(5), 671-678. doi:Doi 10.1175/1520-0485(1976)006<0671:Eoaops>2.0.Co;2

Weber, E. D., Auth, T. D., Baumann-Pickering, S., Baumgartner, T. R., Bjorkstedt, E. P., Bograd, S. J., Burke, B. J., Cadena-Ramírez, J. L., Daly, E. A., de la Cruz, M., Dewar, H., Field, J. C., Fisher, J. L., Giddings, A., Goericke, R., Gomez-Ocampo, E., Gomez-Valdes, J., Hazen, E. L., Hildebrand, J., Horton, C. A., Jacobson, K. C., Jacox, M. G., Jahncke, J., Kahru, M., Kudela, R. M., Lavaniegos, B. E., Leising, A., Melin, S. R., Miranda-Bojorquez, L. E., Morgan, C. A., Nickels, C. F., Orben, R. A., Porquez, J. M., Portner, E. J., Robertson, R. R., Rudnick, D. L., Sakuma, K. M., Santora, J. A., Schroeder, I. D., Snodgrass, O. E., Sydeman, W. J., Thompson, A. R., Thompson, S. A., Trickey, J. S., Villegas-Mendoza, J., Warzybok, P., Watson, W., & Zeman, S. M. (2021). State of the California Current 2019–2020: Back to the Future With Marine Heatwaves? *Frontiers in Marine Science, 8*(1081). doi:10.3389/fmars.2021.709454

Wen, C. H., Kumar, A., & Xue, Y. (2014). Factors contributing to uncertainty in Pacific Decadal Oscillation index. *Geophysical Research Letters, 41*(22), 7980-7986. doi:10.1002/2014gl061992

Zaba, K. D., & Rudnick, D. L. (2016). The 2014-2015 warming anomaly in the Southern California Current System observed by underwater gliders. *Geophysical Research Letters, 43*, 1241-1248. doi:10.1002/2015GL067550

Zhang, Y., Wallace, J. M., & Battisti, D. S. (1997). ENSO-like interdecadal variability: 1900-93. *Journal of Climate, 10*, 1004-1020.

Chapter 2: Observations of Anomalous Oxygen Concentration from the California Underwater Glider Network

Abstract

The California Underwater Glider Network (CUGN) has continuously monitored the California Current Ecosystem (CCE) with Spray underwater gliders since 2005, including dissolved oxygen concentration since 2017. An important result of these measurements is the computation of the mean annual cycle of dissolved oxygen over a multi-year period and the associated anomaly field from this mean. Here we provide a first look at the anomaly of dissolved oxygen concentration from CUGN. This study analyzes salinity, oxygen, and depth on an isopycnal, or constant density surface, and salinity at a constant depth to understand the cause of anomalous periods of oxygen concentration. We find that a major contributing factor is changes in source water concentration due to westward propagating Subthermocline Eddies (STEs).

Introduction

The California Underwater Glider Network (CUGN) is a sustained effort to observe variability in the California Current Ecosystem (CCE) using a fleet of autonomous ocean profilers known as Spray underwater gliders (Rudnick et al., 2017). These gliders make repeated dives from the surface to 500 m and back, traveling approximately 3 km in the process. Each glider is equipped with a suite of sensors to measure temperature, pressure, salinity, acoustic backscatter, chlorophyll fluorescence, and velocity. The data are processed for quality and gridded with an objective mapping procedure to produce a product with a spatial resolution of 10 meters in depth (10 - 500 meters), 5 kilometers in distance (5 - 530 kilometers offshore), and a temporal resolution of 10 days (2005 - present). The three primary CUGN lines are identical to those used in the historic California Cooperative Fisheries Investigation (CalCOFI) research

program, line 66.7, off Monterey Bay, line 80, off Point Conception, and line 90, off Dana Point (Figure 2.1). In this study data from CUGN is used to create high resolution climatologies of the CCE from 2017 to present that include novel dissolved oxygen concentration data. The results analyze anomalies from the annual cycle and provide possible explanations for the causality of these events.

Overview of the California Current Ecosystem

Figures 2.1-2.7 below lay out the physical dynamics of the CCE, in terms of mean geostrophic flow and seasonal upwelling cycle, as represented by the mean depth of an isopycnal, or constant density surface.

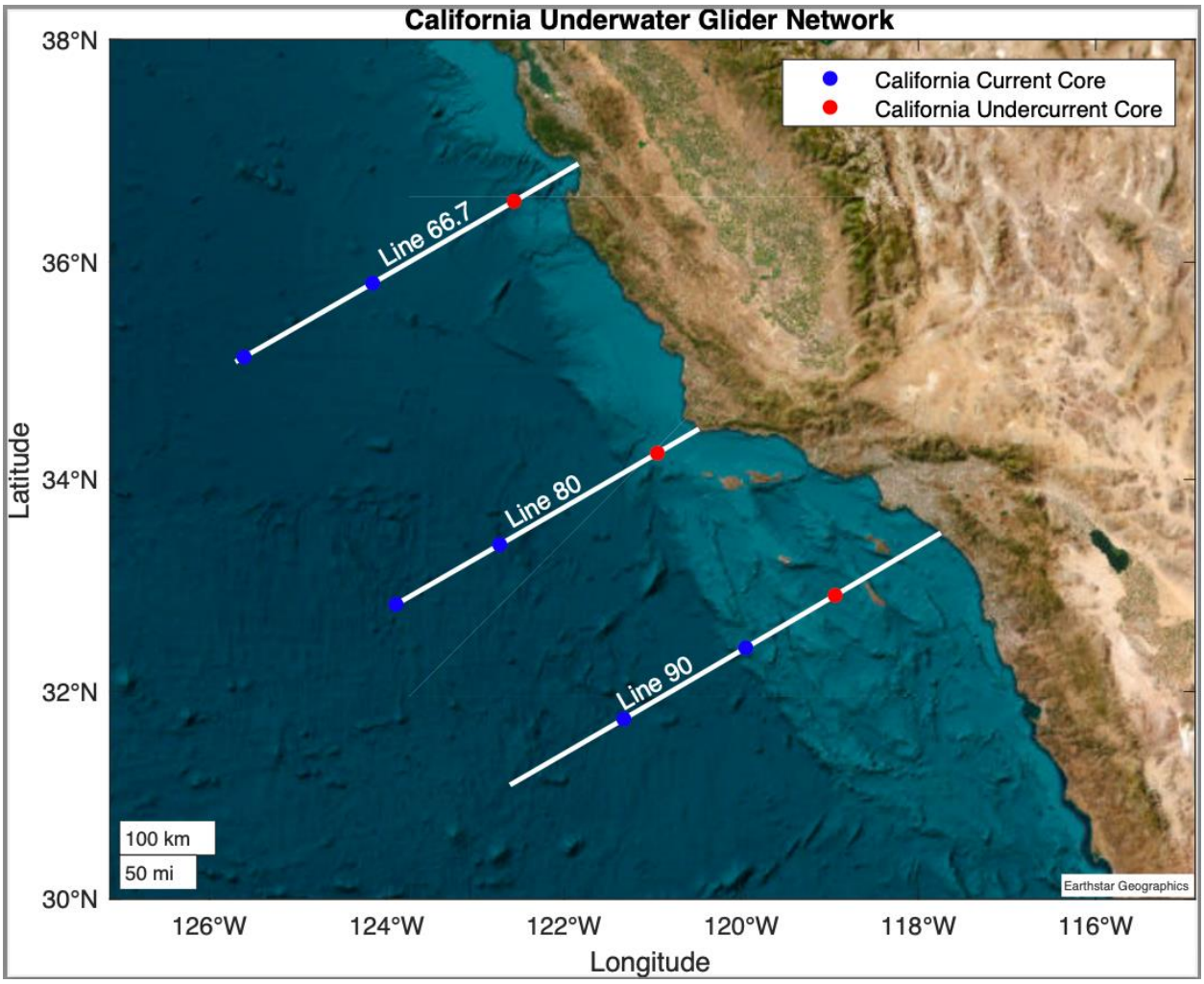

Figure 2.1 California Underwater Glider Network lines (white) and geostrophic current cores (blue circles - northward flow) and (red circles - southward flow). Line 66.7 is off Monterey Bay, California and extends from 0 - 400 km offshore. Line 80 is off Point Conception, California and extends from 0 - 365 km offshore. Line 90 is off Dana Point, California and extends from 0 - 530 km offshore.

The California Undercurrent (CU) flows northward and introduces high temperature, high salinity, low oxygen water, or Pacific Equatorial Water (PEW), into the CCE (Bograd et al., 2019). The CU extends from approximately 150 km offshore of lines 66.7 and 90, and approximately 125 km offshore of line 80. The California Current (CC) flows southward and introduces Pacific Subarctic Upper Water (PSUW), low temperature, low salinity, and high oxygen water, into the CCE (Bograd et al., 2019). The CC extends approximately 150 km offshore to the edge of the glider profiles on all three lines. There are typically two main cores where the CC is strongest (Rudnick et al., 2017) (Figures 2.2-2.3). Upwelling in the CCE typically occurs in the spring season because the net transport of water from alongshore winds is offshore. This process causes isopycnal surfaces to shoal, which can be measured over time as a metric for upwelling. A full description of the CCE is documented by (Rudnick et al., 2017).

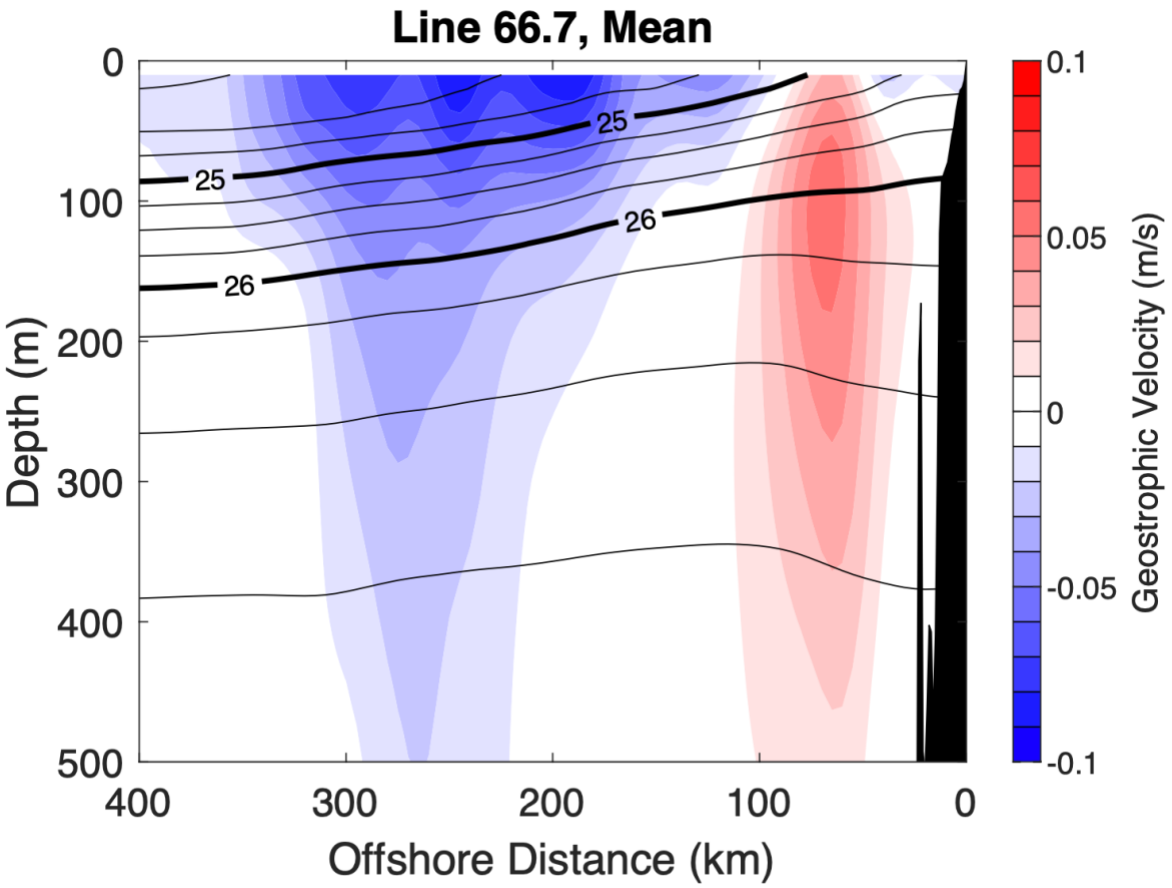

Figure 2.2 Mean geostrophic velocity line 66.7. Isopycnal surfaces are depicted as black contour lines. The positive (red) values represent northward flow, indicative of the California Undercurrent. The negative (blue) values represent southward flow, indicative of the California Current. Geostrophic flow is strongest in the CU near isopycnal 26.0 (75-150 m) and in the CC above the 25.0 isopycnal (10-50 m). Topography is masked in black.

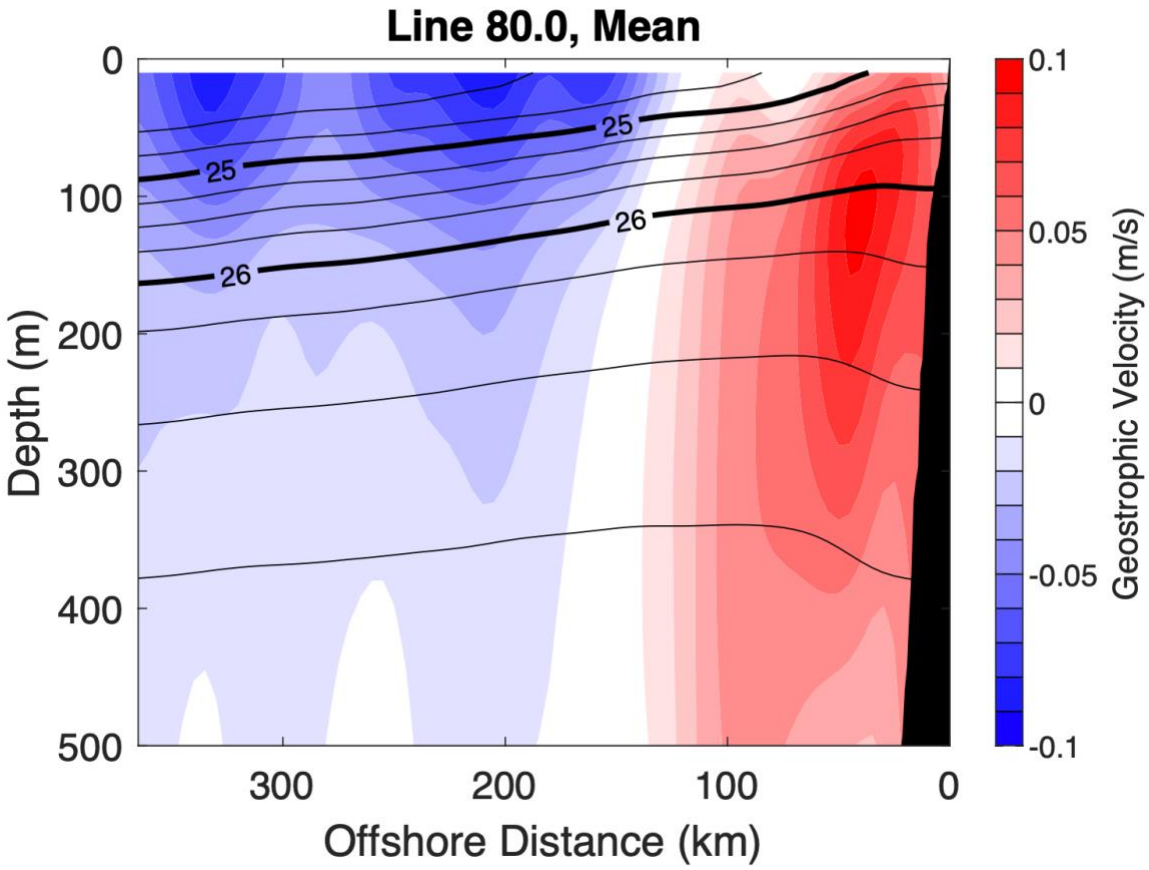

Figure 2.3 Like figure 2.2, line 80.

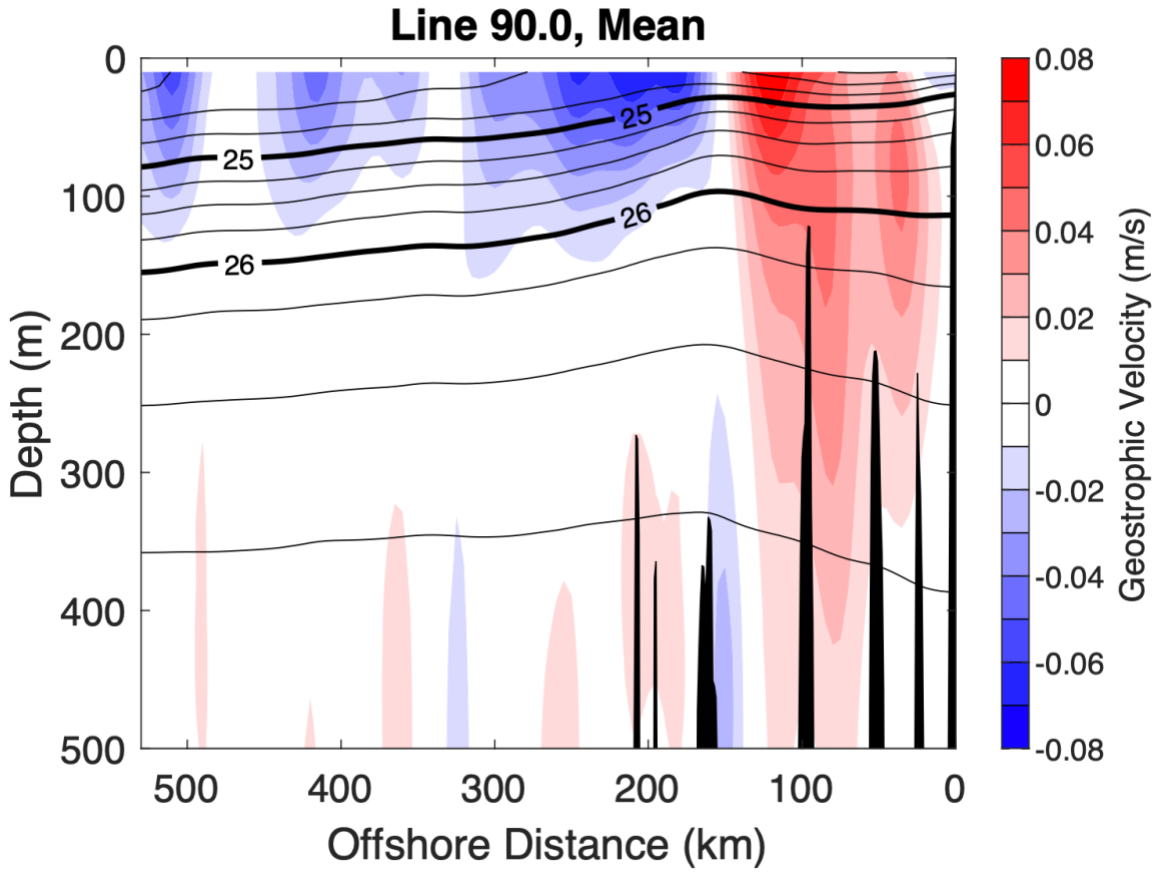

Figure 2.4 Like figure 2.2, line 90. Geostrophic flow is strongest in both the CU and the CC near isopycnal 25.0 (75-150 m).

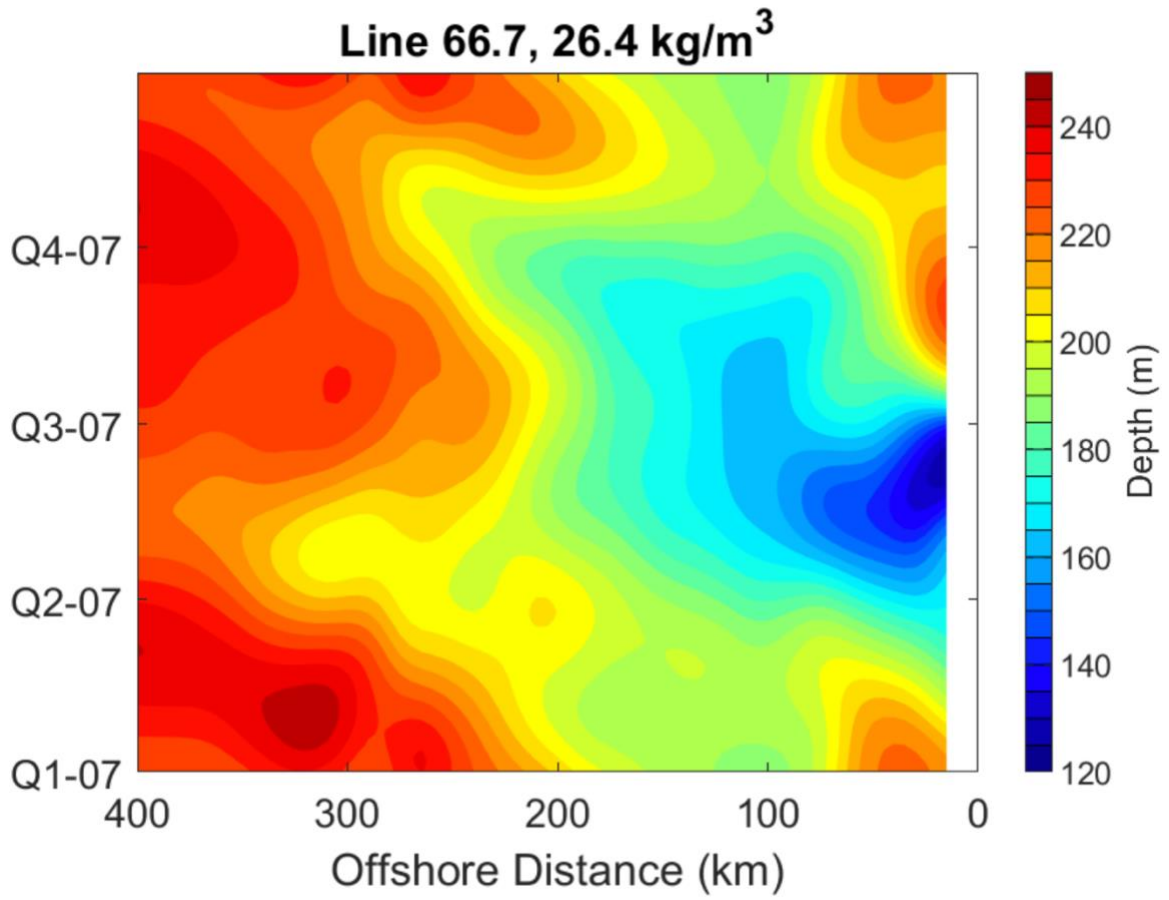

Figure 2.5 Mean annual cycle of the 26.4 kg/m^3 isopycnal surface, representing the seasonal upwelling cycle on line 66.7. During the spring season, the isopycnal surface shoals inshore as upwelling pumps water from depth to the surface. Blue depicts a shallower depth, red depicts a greater depth.

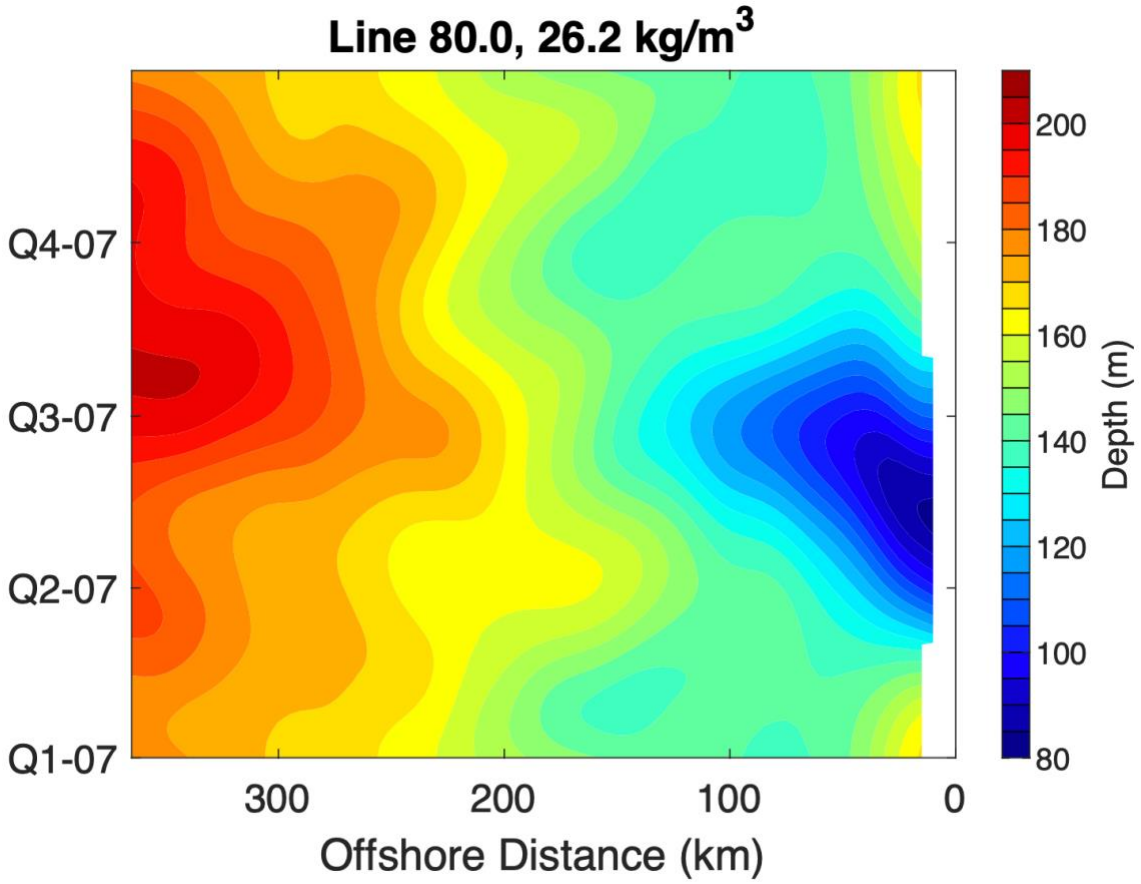

Figure 2.6 Like figure 2.4, line 80, isopycnal 26.2.

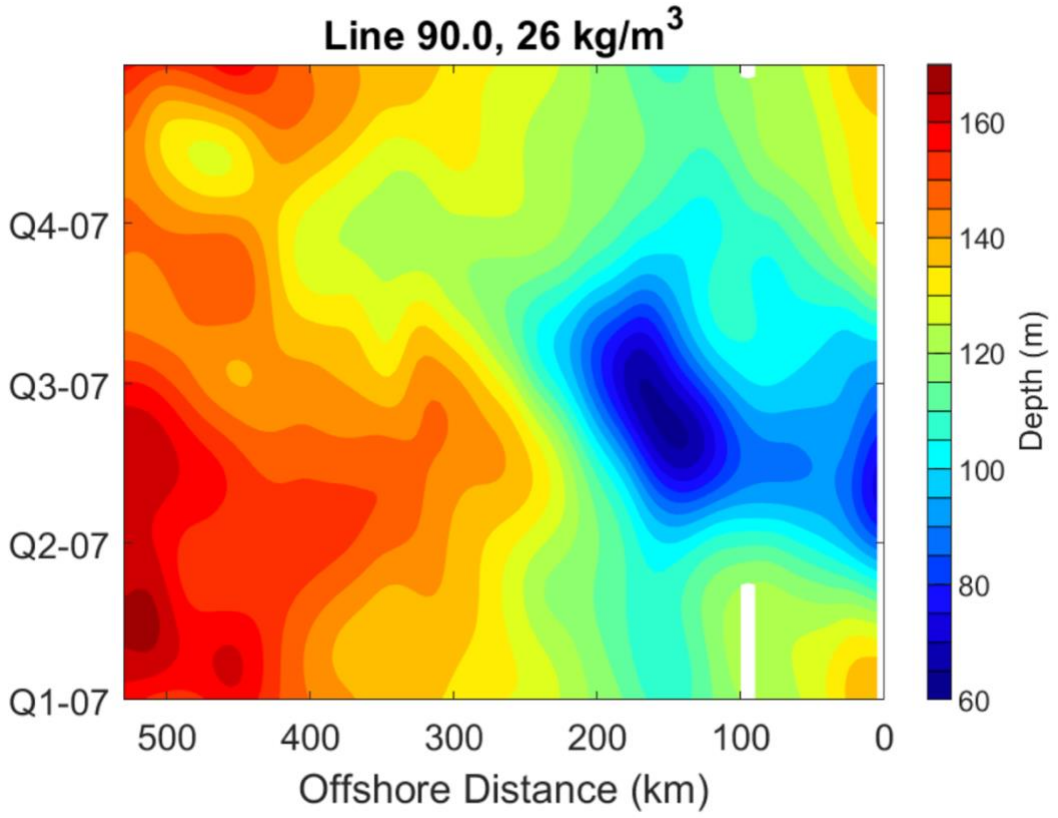

Figure 2.7 Like figure 2.4, line 90, isopycnal 26.0. Upwelling extends farther offshore on line 90 than lines 80 and 66.7.

Data and Methods

The California Underwater Glider Network lines 66.7, 80, and 90 are used for this project. The period from January 1, 2017 - December 31, 2022, is chosen for availability of dissolved oxygen (DO) concentration data. The DO time series was interrupted in mid 2017 on line 90 and in mid 2020 on line 66.7 due to instrumentation issues. The full methods for the CUGN climatology are described extensively by Rudnick et al. (2017), this section will cover the main processes used to calculate the mean annual cycle and anomaly from the annual cycle for this analysis.

Data from each glider is first quality controlled and averaged into evenly spaced bins from 10 m to 500 m in the vertical dimension, with approximately 12 samples per bin. The annual cycle is then calculated for each discrete grid point at 5 km intervals by fitting one constant and three harmonics to the data using a least-squares fit. The distance along each line is calculated by projecting onto the CalCOFI coordinate system and the results are weighted to filter out the effects of high-frequency variability according to equation 1. Data resulting in w(x) being smaller than 0.001 are not used. The annual cycle is computed for the entire time period, 2017- 2022 inclusive.

$$w(x) = \exp(-x^2/L^2)$$

Equation 1. x is distance offshore. L is the e-folding length scale.

The annual cycle is subtracted from the data and an objective mapping procedure is used to compute the anomaly. The covariance matrix is specified as a function of lags in distance and time, or autocorrelations, then calculated at each depth and averaged over all three lines. A two-dimensional Gaussian window is fit to these autocorrelations at lags less than 200 days and 200 km and the e-folding scale is found to be 60 days and 100 km. An e-folding scale of 60 days and

30 km is chosen to reduce the effects of smoothing, with negligible effects on the resulting map (Rudnick et al., 2017). The final product is a three-dimensional gridded data set with a resolution of 10 meters depth x 5 kilometers distance x 10 days. The absolute geostrophic velocity can be computed from the objective map using the thermal wind relationship to obtain the vertical shear and referencing this with the across-section depth-average current velocity (Ren & Rudnick, 2022; Rudnick et al., 2017).

For the analysis, an isopycnal surface relevant to the upwelling and thermocline depth is chosen for each line. These are the 26.0 kg/m^3 isopycnal surface for line 90, the 26.2 kg/m^3 isopycnal surface for line 80, and the 26.4 kg/m^3 isopycnal surface for line 66.7. Isopycnal surfaces that indicate upwelling increase with more northern lines, as the water is generally cooler and shallower isopycnals will reach the surface and outcrop from data records.

Results

Hovmoller diagrams are created for DO, salinity, and depth on each line for their respective isopycnal surfaces. This process is repeated with the anomalies from the annual cycle. Two hypotheses are then presented to explain the anomalous periods of dissolved oxygen from the annual cycle. The first is that source water controls oxygen concentration in the CCE, and departures from the annual cycle imply either more PSUW or PEW in the system. Source waters have distinct characteristics and can be distinguished by salinity as measured on an isopycnal. This quantity is known as a tracer because it is conserved as the water mass advects horizontally. The advantage of mapping on an isopycnal surface is that the impacts of heaving (up and down motion) are removed. The second hypothesis is that anomalous oxygen events are caused by upwelling. This quantity can be measured by calculating the depth of an isopycnal surface, where a shallower isopycnal implies increased upwelling and a deeper isopycnal implies more

downwelling (less upwelling). It is more advantageous, however, to use depth surfaces to study upwelling as isopycnal surfaces remove most of the impact. To further examine the effects of upwelling, oxygen-salinity joint-pdfs are created at a constant depth surface of 50 m.

Part I: Climatology: Dissolved Oxygen, Salinity, and Isopycnal Depth in the California Current Ecosystem

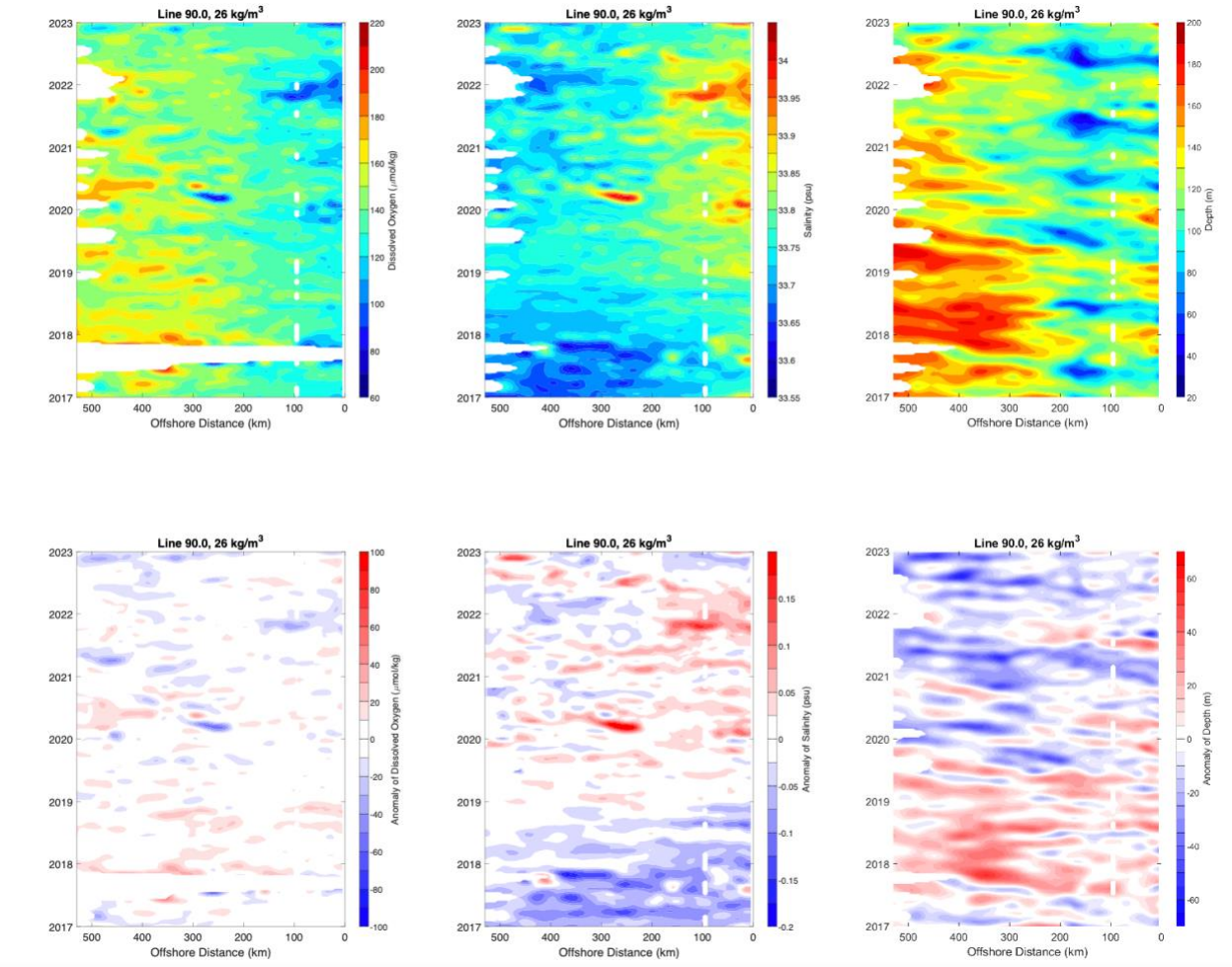

Figure 2.8 Line 90, Isopycnal 26.0 kg/m^3. X-axis is offshore distance, Y-axis is time, the color contours from left to right display dissolved oxygen concentration, salinity, and depth of the isopycnal surface. The top three figures are the total measured values, and the bottom three figures are the anomalies from the annual cycle. DO records are unavailable on line 90 during several months in 2017 as well as the vertical white line near 100 km.

The seasonal cycle of upwelling inshore of 200 km is the most striking signal in the total plots for oxygen, salinity, and depth. During spring months, March-May, there is a clear shoaling of the isopycnal surface accompanied with higher salinity and lower oxygen. Offshore of 200 km, the isopycnal surface deepens, especially in the earlier period of the record. Over this entire

line and period, salinity and oxygen are highly related on the isopycnal surface, though not entirely identical. At the end of the Southern California Bight, around 200 km offshore (Rudnick et al., 2017), there is a stark contrast in DO, salinity, and depth of isopycnal surface where the CC and CU meet. This agrees with the mean geostrophic velocity in this region (Figures 2.2-2.4). Over the entire period and line, there are trends of a shoaling isopycnal depth, increasing salinity, and decreasing oxygen. This could be due to an increasing amount of PEW in the California Current and Undercurrent or upwelling inshore. A notable low oxygen anomaly occurred inshore in late 2021 and propagated offshore until early 2022. This same pattern is reflected as a high anomaly in the salinity record. An explanation could be the across-shore propagation of subthermocline eddies (STEs) identified as salinity or oxygen anomalies along an isopycnal that propagate horizontally. These eddies are known to significantly affect mixing and transport of biogeochemical tracers in the CCE region (Frenger et al., 2018; Ren & Rudnick, 2022).

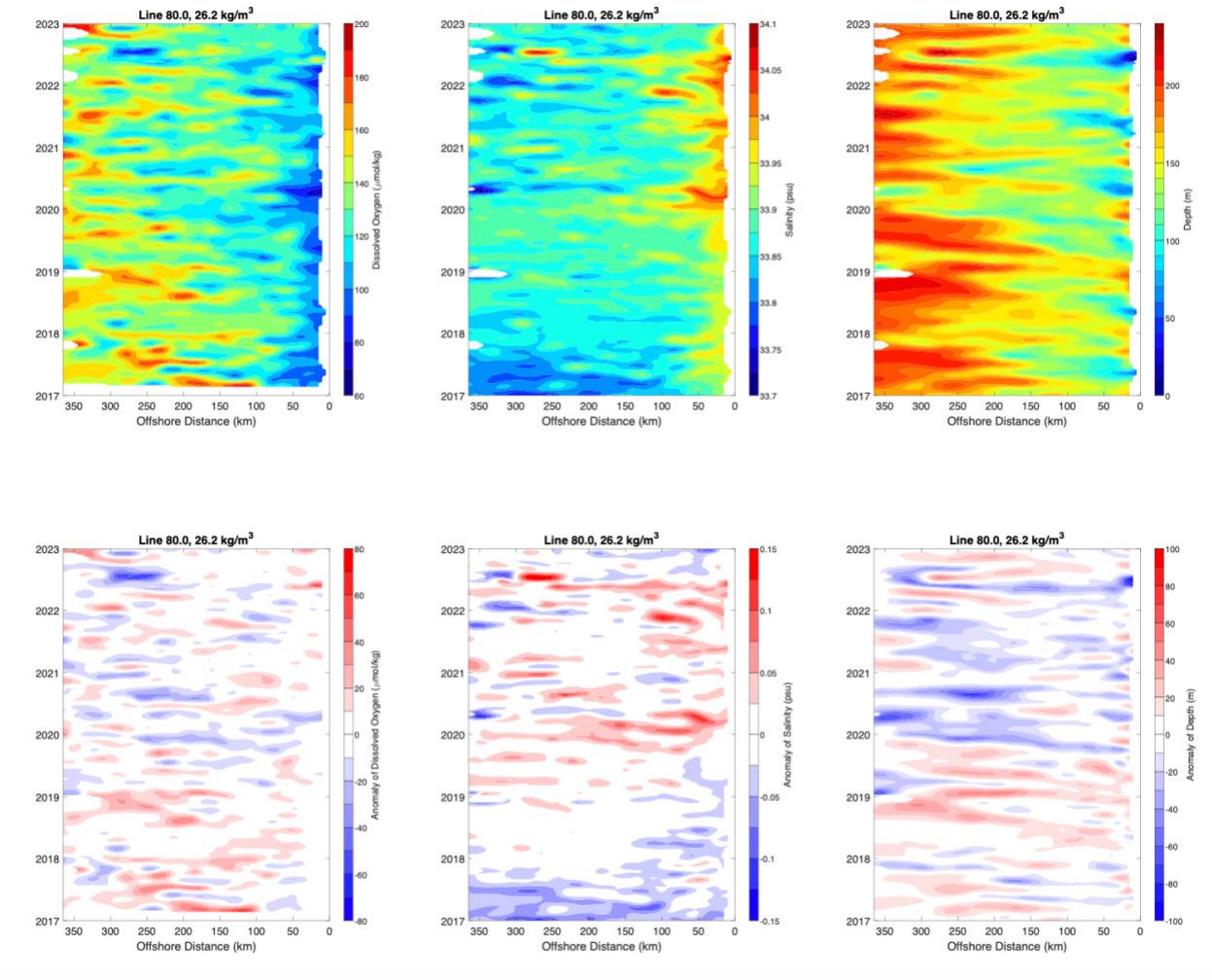

Figure 2.9 Like figure 2.8, on line 80, isopycnal surface 26.2 kg/m^3.

On line 80, there is a strong seasonal upwelling signal extending approximately 150 km offshore, where the isopycnal surface rapidly deepens. The upwelling signal is generally strongest inshore of 50 km. For this inshore region, there is a clear trend of increasing salinity along with shoaling isopycnal depth that is further reflected in the anomaly plots. Previously Ren and Rudnick (2021a) found that the California Current was a source of high salinity water from 2017-2019 that advected from offshore to the coast. Another possible explanation for this high salinity period could be strengthened upwelling, though the trend is not so clearly reflected in the oxygen record. In 2017, the entire region experienced a period of low salinity accompanied in

the offshore region by a deeper isopycnal and higher oxygen concentration, though inshore the opposite is true. This low salinity period continues inshore through mid 2019 along with a period of high oxygen and a deep isopycnal surface. In mid 2018, near 200 km offshore, a period of high oxygen propagates out to 350 km offshore lasting until early 2019. Interestingly, the salinity record remains near its mean value and the isopycnal is deeper than normal. This event is likely due to an influx of PSUW in the CC region. In late 2019, there is a characteristic STE event where a high salinity and low oxygen anomaly begins 50 km offshore and propagates outward to the end of the glider line.

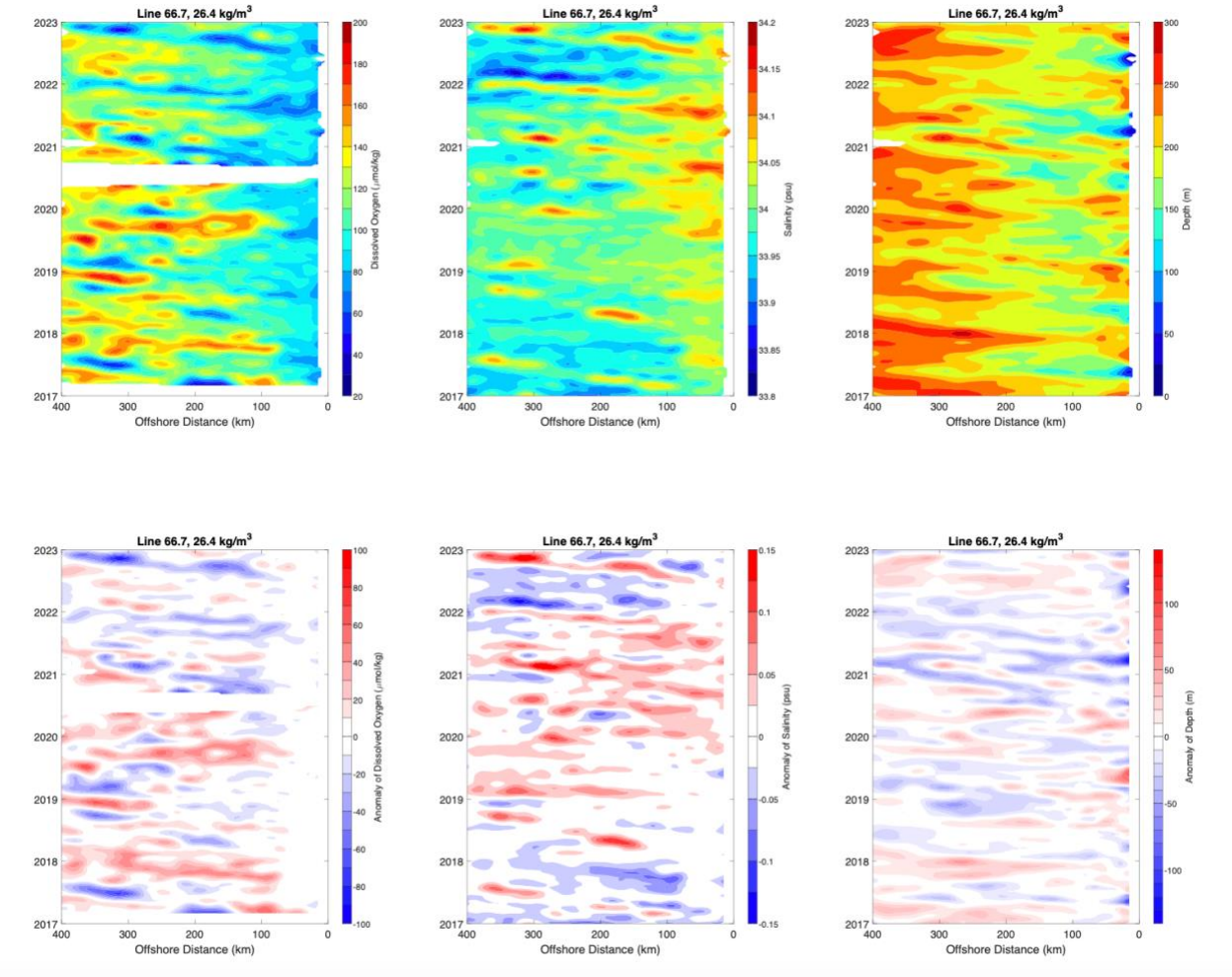

Figure 2.10 Like figure 2.8, on line 66.7, isopycnal surface 26.4 kg/m^3.

On line 66.7 at isopycnal 26.4, the upwelling signal is strongest inshore of 50 km, though it extends to approximately 125 km. Over this period there is an increasing trend of upwelling apparent in the shoaling isopycnal, increase in salinity, and decrease in DO. There are two major periods of anomalously high oxygen concentration during this record. The first begins in late 2017, 100 km offshore and propagates outward to 400 km until mid 2018. During this period, salinity was lower and the isopycnal was deeper than normal. The second period begins in mid 2019, around 100 km and again propagates outward to 400 km lasting until early 2020. This time however, the salinity record was higher than normal and the isopycnal surface was both positive and negative over this region. The cause of these high oxygen anomaly events is still unclear. In this period, there are three major low oxygen concentration anomalies that all follow a similar characteristic pattern of across-shore STEs. In late 2020, late 2021, and late 2022 to early 2023 a low oxygen anomaly begins approximately 100 km offshore and propagates offshore to 400 km. Notably during each of these three events there was also a high salinity anomaly. The influence of STEs is further investigated in part II.

Part II: Investigating Oxygen Anomalies in the CCE

To further investigate the two hypotheses presented above, joint pdfs are calculated on isopycnal surfaces for oxygen-layer thickness, salinity-layer thickness, dissolved oxygen-salinity, and on a depth surface for dissolved oxygen-salinity pairs. These are calculated for an inshore region of 0-200 km and offshore of 200 km to the end of the CUGN line during the entire record. The purpose is to determine the joint distribution of these variable pairs. Layer thickness is measured as the distance in meters between the 25.7 and 26.8 isopycnal surface, and serves as a proxy for stratification, and has previously been used as an indicator of STEs where a thicker layer is associated with lower DO and higher salinity (Ren & Rudnick, 2022). A negative relationship for oxygen-salinity on an isopycnal surface is expected because high salinity typically corresponds with low oxygen (PEW mass) and low salinity typically correspond with high oxygen (PSUW mass). On a depth surface for dissolved oxygen-salinity, a negative relationship is expected inshore due to upwelling and no relationship is expected offshore. The oxygen-layer thickness relationship is expected to be negative inshore and offshore because low oxygen concentration will correspond with a thicker layer due to the presence of STEs and vice versa (Ren & Rudnick, 2022). The calculation is performed on the anomaly map to remove the impacts of the seasonal cycle.

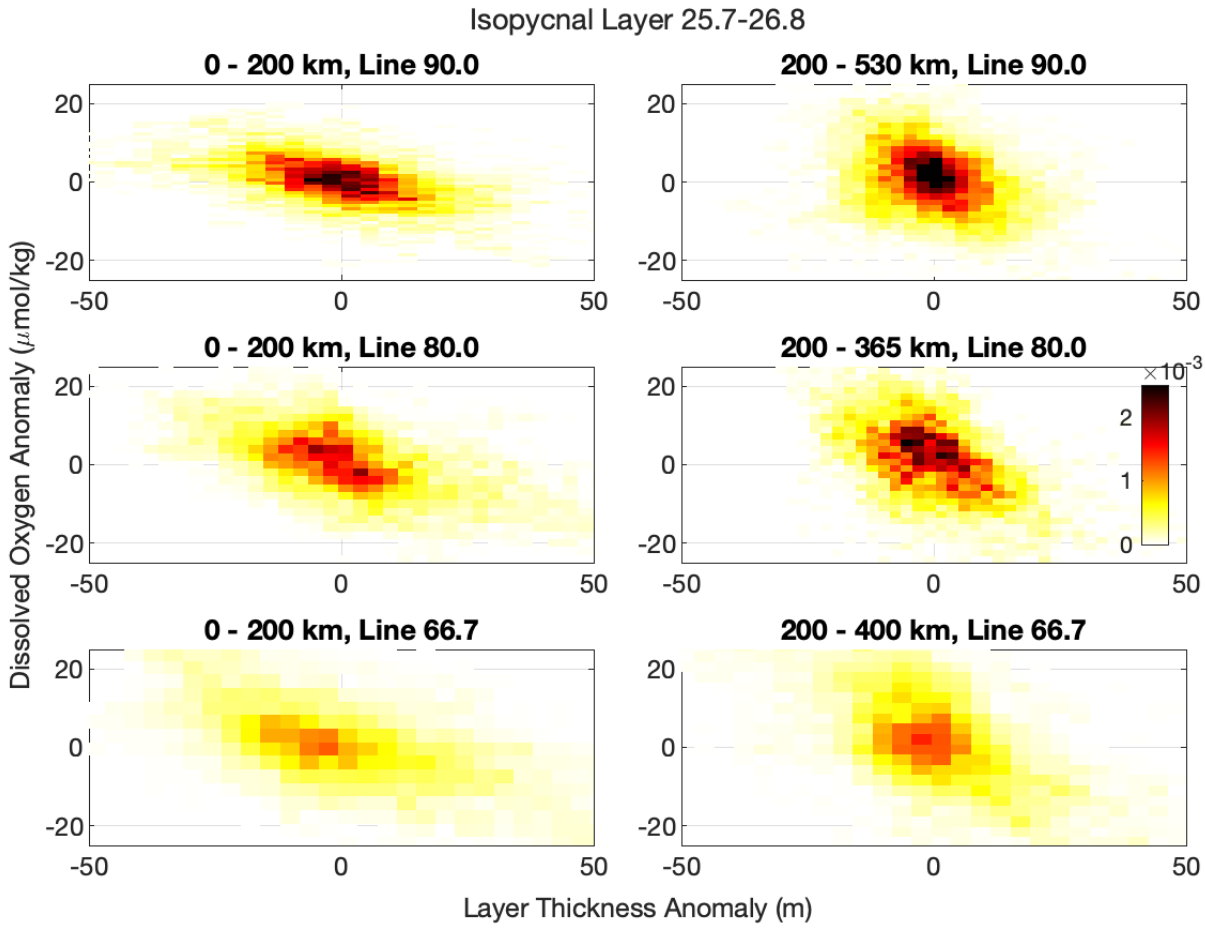

Figure 2.11 The x-axis is the anomaly of layer thickness from the annual cycle defined as the distance between the 25.7 and 26.8 isopycnal surfaces on the anomaly map. The y-axis is the mean anomaly dissolved oxygen concentration for the defined layer. Oxygen anomaly and layer thickness anomaly are negatively correlated and dependent.

Dissolved oxygen and layer thickness are negatively correlated and dependent both inshore and offshore for all three lines. Inshore, the correlation is stronger than offshore, a feature that is consistent with the fact that STEs propagate PEW westward into the CC region.

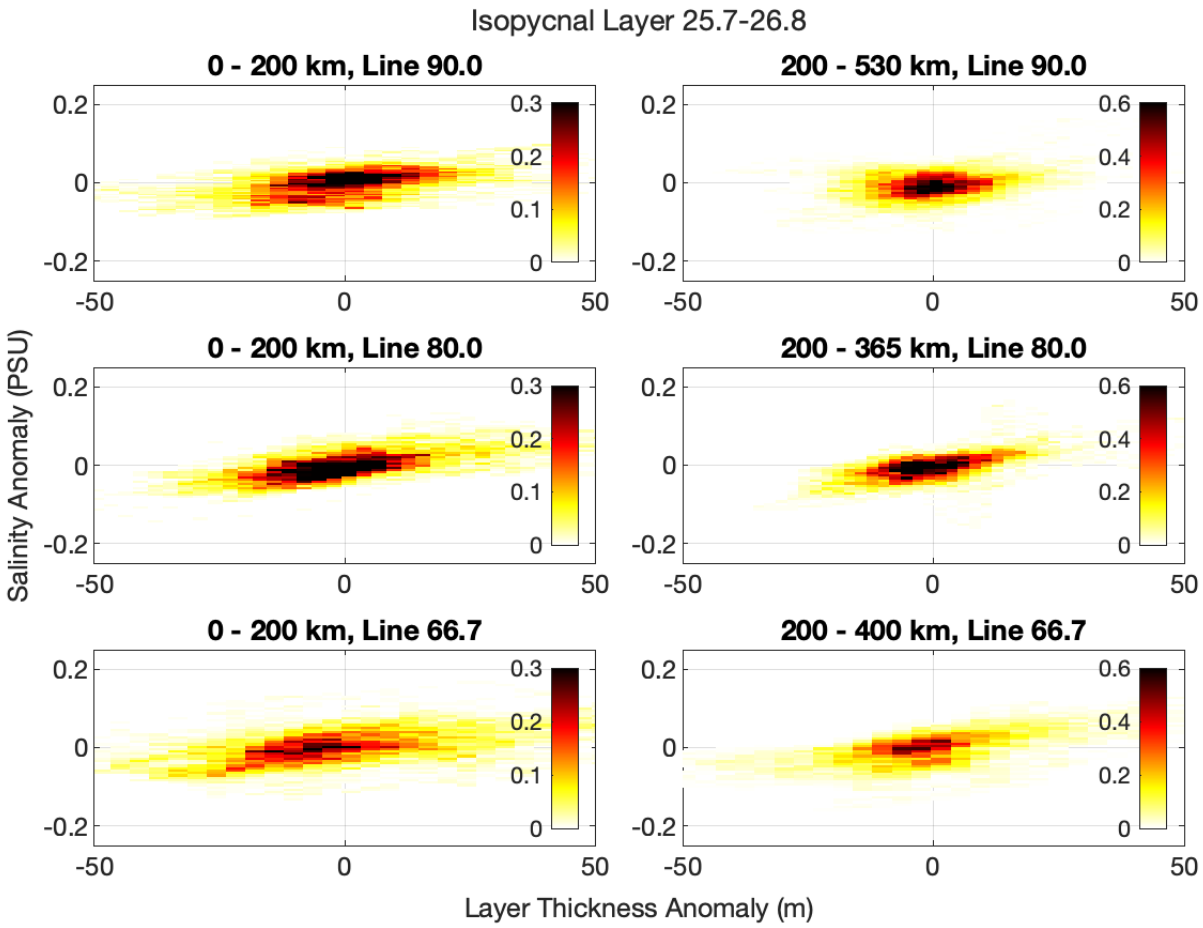

Figure 2.12 The y-axis is the mean salinity anomaly between isopycnal 25.7 and 26.8, and x-axis is the layer thickness anomaly between the same two isopycnal surfaces. Salinity anomaly and layer thickness anomaly are positively correlated and dependent.

Both inshore and offshore, salinity and layer thickness are positively correlated and dependent on all three lines. Inshore, the distribution of layer thickness is wider than offshore.

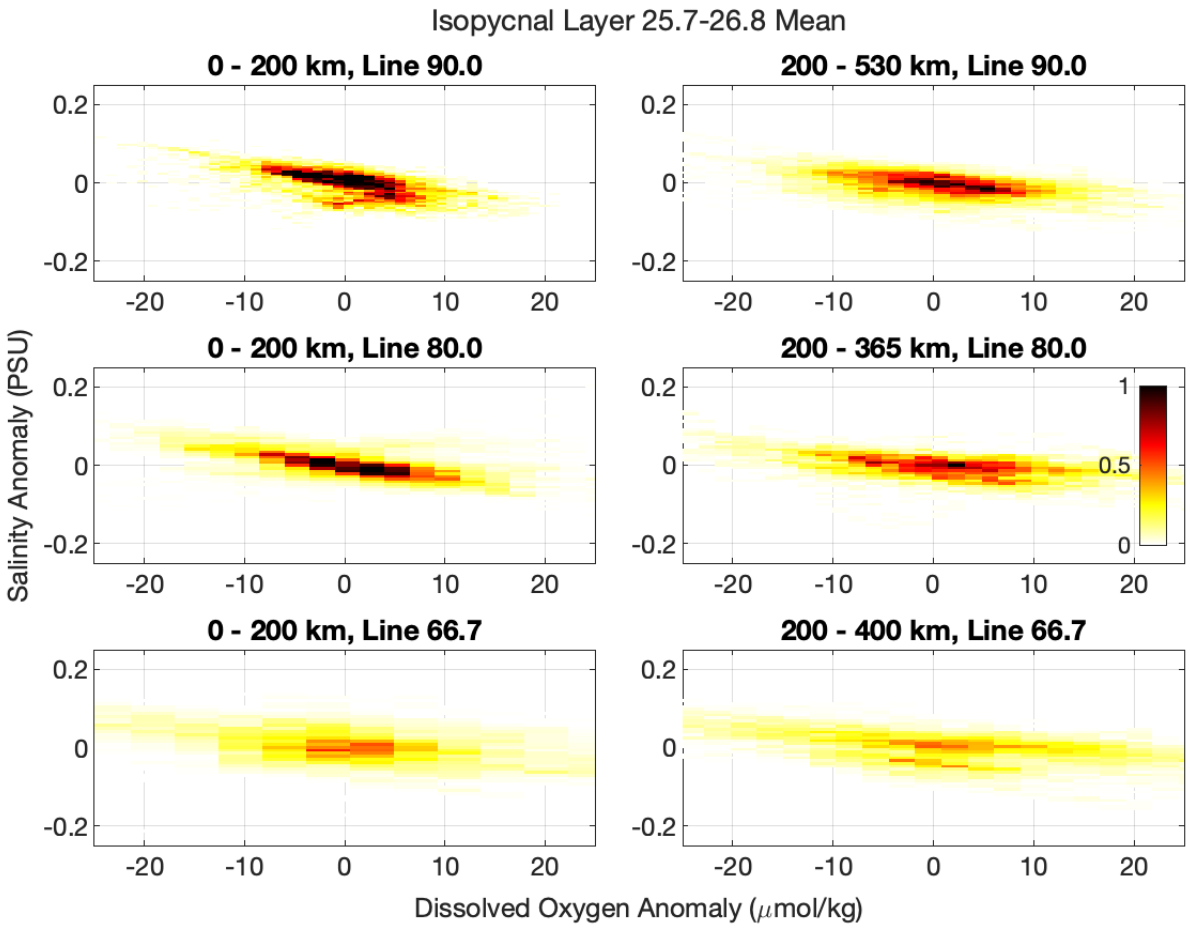

Figure 2.13 like figure 2.12, for salinity and dissolved oxygen anomaly on isopycnal surfaces. Title reads: line – region – isopycnal.

For all three lines, both inshore and offshore, oxygen and salinity are negatively correlated and dependent. The negative relationship is likely because high salinity-low oxygen properties are associated with PEW and low salinity-high oxygen properties are associated with PSUW.

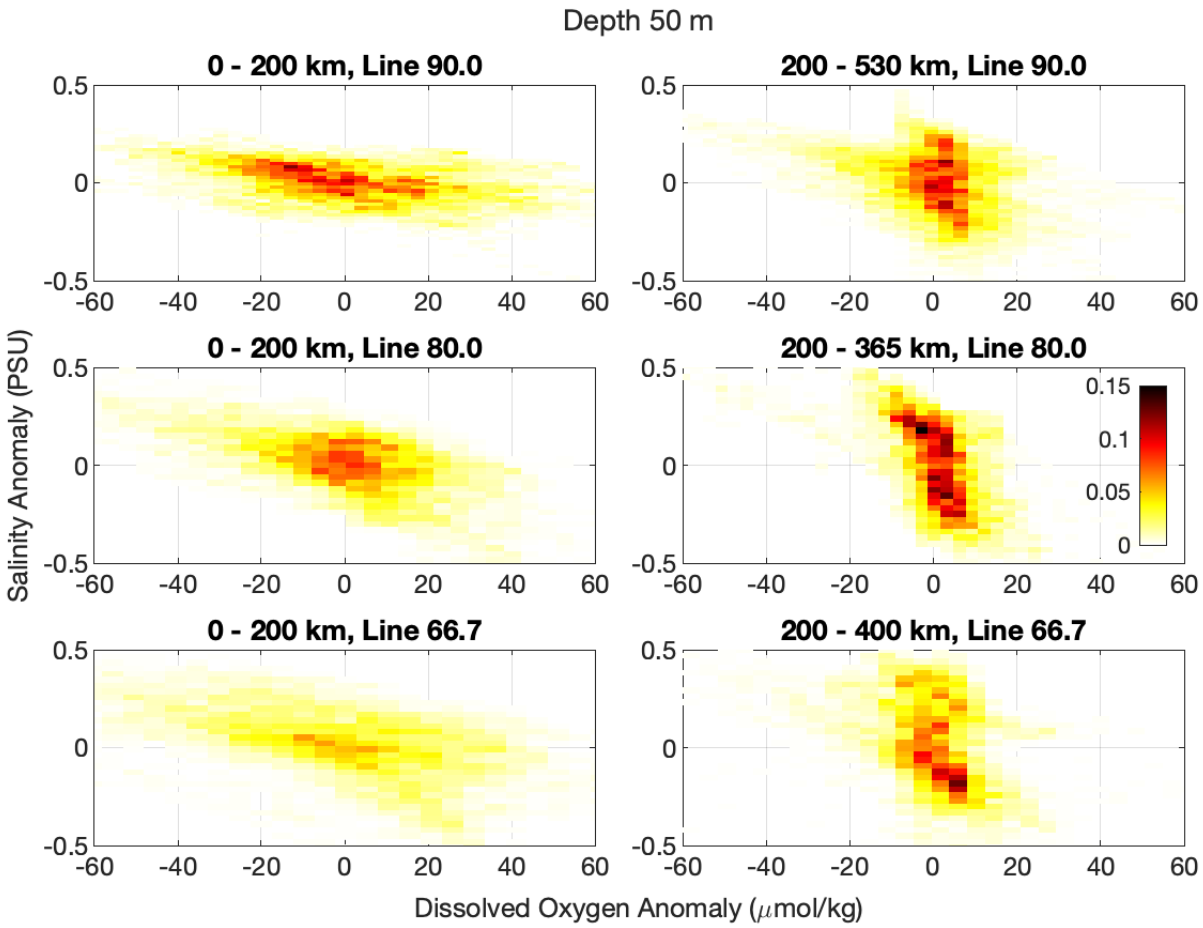

Figure 2.14 Like Figure 2.13, for salinity and dissolved oxygen anomaly at a constant depth surface. Title reads: line – region – depth.

For all three lines, inshore, there is a negative correlation between oxygen and salinity indicative of upwelling. Offshore, however, the joint distribution is nearly vertical (slightly negative), meaning that there is a weak relationship between the two variables. The impacts of upwelling are included in this plot, as this is measured at a constant depth of 50 meters rather than on a constant isopycnal. The full extent of the upwelling process observed at 50 m causes a much greater range of salinity and dissolved oxygen values then are observed on a constant isopycnal surface.

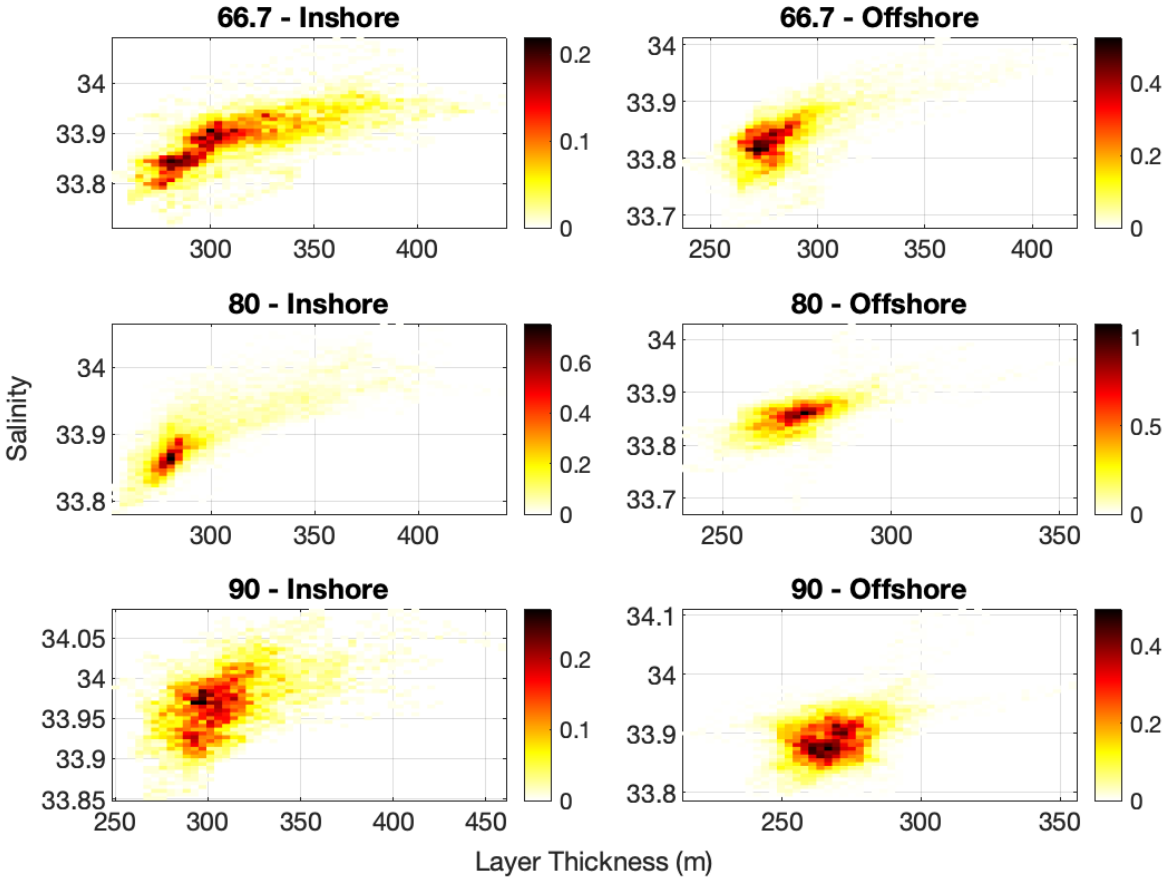

Figure 2.15 Like figure 2.12, for total measured value. Salinity and layer depth have a positive non-linear correlation and are dependent.

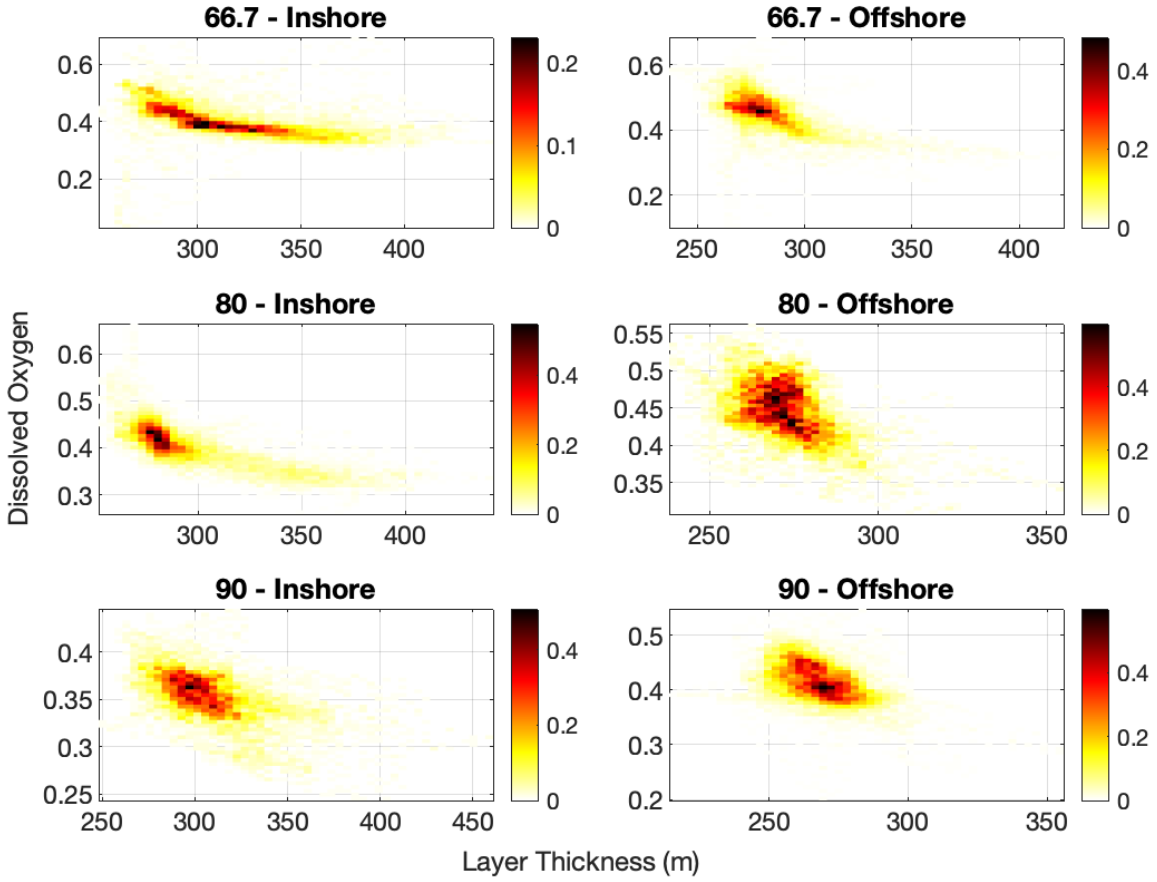

Figure 2.16 Like figure 2.11, for total measured value. Oxygen and layer depth have a negative non-linear correlation and are dependent.

Discussion

The significance of this chapter is a first look at the anomaly of dissolved oxygen concentration from the annual cycle. In part one, anomalous periods were identified and examined alongside salinity and the depth of an isopycnal surface. Part two examined the joint distributions between oxygen, salinity, depth, and layer thickness to understand how upwelling and source water each contribute to anomalous oxygen events. There are two key takeaways from this analysis: (1) The negative correlation of dissolved oxygen and salinity anomalies suggest that changes in source water are important factors. (2) Across-shore subthermocline eddies are a fundamental cause of low oxygen – high salinity anomalies in the California Current Ecosystem.

That dissolved oxygen and salinity anomalies have such a strong and negative correlation highlights the importance of the PEW and PSUW water masses to biological tracers in this region. This is highlighted by the joint-pdfs in figure 2.13, which reveal that on all three lines for an isopycnal surface the oxygen-salinity correlation was negative both inshore and offshore, suggesting that oxygen concentration anomaly has a relationship with source water. On a constant depth surface, however, the impacts of upwelling are included and there was only a negative correlation for the inshore region. The second key takeaway is that the across-shore propagation of STEs is a fundamental cause of oxygen anomalies in the CCE. These eddies transport high salinity, low oxygen PEW from the California Undercurrent westward into the California Current region. The influence of these events is especially clear in figure 2.10 as DO or salinity anomalies on line 66.7 that tilt offshore overtime. The joint pdfs in figures 2.11 and 2.12 also suggest that both oxygen and salinity anomalies are dependent on layer thickness anomalies. In figure 2.11, oxygen and layer thickness are negatively correlated, though a

stronger correlation is found inshore. For the salinity-layer thickness joint pdf in figure 2.12, a similar pattern is found for the inshore and offshore region, however, with a positive correlation. These results strongly agree with Ren and Rudnick (2022), and confirm this for the anomaly field as well.

The California Current Ecosystem is a highly dynamic and productive region where oxygen concentration has extensive biological implications. Through this analysis of anomalies from the annual cycle with novel dissolved oxygen concentration data from the CUGN, we confirm that source water is a major factor for changes in oxygen concentration and that low oxygen-high salinity anomalies are likely a result of across-shore STEs. Future research in this area should continue to examine the reason for high oxygen anomalies. Some possible explanations could be decreased upwelling, advection of the PSUW mass to the inshore region, or even biological factors. Subthermocline eddies are truly fantastic processes that can advect significant amounts of water in the across-shore direction and have large effects on the region. Continued research could improve biogeochemical ocean models and improve our understanding of the California Current Ecosystem.

References

Bograd, S. J., Schroeder, I. D., & Jacox, M. G. (2019). A water mass history of the Southern California current system. *Geophysical Research Letters, 46*(12), 6690-6698. doi:10.1029/2019gl082685

Frenger, I., Bianchi, D., Stuhrenberg, C., Oschlies, A., Dunne, J., Deutsch, C., Galbraith, E., & Schutte, F. (2018). Biogeochemical Role of Subsurface Coherent Eddies in the Ocean: Tracer Cannonballs, Hypoxic Storms, and Microbial Stewpots? *Global Biogeochemical Cycles, 32*(2), 226-249. doi:10.1002/2017gb005743

Ren, A. S., & Rudnick, D. L. (2021). Temperature and salinity extremes from 2014-2019 in the California Current System and its source waters. *Communications Earth & Environment, 2*(1). doi:ARTN 62
10.1038/s43247-021-00131-9

Ren, A. S., & Rudnick, D. L. (2022). Across-Shore Propagation of Subthermocline Eddies in the California Current System. *Journal of Physical Oceanography, 52*(1), 39-51. doi:10.1175/Jpo-D-21-0137.1

Rudnick, D. L., Zaba, K. D., Todd, R. E., & Davis, R. E. (2017). A climatology of the California Current System from a network of underwater gliders. *Progress in Oceanography, 154*, 64-106. doi:10.1016/j.pocean.2017.03.002

Chapter 3: Environmental Factors on Ichthyoplankton Abundance in the California Current Ecosystem

Abstract

As basin-wide climate indices become less effective due to rapid changes in climate, the value of localized metrics increases. Sea surface temperature (SST) is a commonly used and spatially continuous measurement of the ocean that is frequently integrated into fisheries stock assessments, however, as many species do not live at the surface, other measurements could prove more useful. Utilizing nearly four decades of ichthyoplankton, or larval fish, abundance data from the California Cooperative Oceanic Fisheries Investigation (CalCOFI) we show that environmental impacts on larval fish abundance can be variable, thus accounting for a broad range of drivers is a critical step in future management. A significant finding of this work is that the larval abundance of several prominent northern and southern mesopelagic species in the California Current Ecosystem (CCE) are highly correlated with a set of environmental conditions that suggest source water is a controlling factor of abundance. Future modeling of fish populations should consider incorporating high resolution data of the CCE, such as the California Underwater Glider Network (CUGN) or CalCOFI, to improve fishery stock assessment.

Introduction

The California Current Ecosystem (CCE) is a highly productive and nutrient rich region in the North Pacific Ocean supported by two opposing currents and a powerful seasonal upwelling cycle. Flowing southward, the California Current (CC) has two main cores (Rudnick et al., 2017) that bring cold, high oxygen, and low salinity, or “minty”, Pacific Subarctic Upper Water (PSUW) (Bograd et al., 2019; Schroeder et al., 2019). Flowing northward, the California Undercurrent (CU) has one main core that brings warm, high salinity, low oxygen, or “spicy”, Pacific Equatorial Water (PEW) (Schroeder et al., 2019). A seasonal spring upwelling cycle,

driven by alongshore winds pumps cold, low oxygen, and high salinity waters from depth up to the surface. These three main processes make for a highly dynamic ecosystem supporting a diverse range of marine life constantly adapting to changing ocean conditions.

This study focuses on the relationships between the two main water masses (PSUW and PEW) and their impacts on larval fish abundance within several major habitats found in the CCE. We hypothesize that in a defined region in which each habitat category (southern mesopelagic, northern mesopelagic, coastal pelagic, and benthic) is found, there will be a unique relationship of environmental conditions to larval abundance. We utilize nearly four decades of California Cooperative Oceanic Fisheries Investigation (CalCOFI) cruise data including temperature, dissolved oxygen concentration, salinity, and ichthyoplankton abundance on lines 90 and 80. Ichthyoplankton, or larval fish, abundance is a commonly used indicator of adult fish population (Koslow et al., 2011; Schroeder et al., 2019). California fisheries are both an important ecological and economic resource in the North Pacific, however, there is a limited understanding of how these species respond to environmental factors other than SST. Therefore, strong correlations between larval abundance and environmental factors could allow high resolution data from CalCOFI or the California Underwater Glider Network (CUGN) to improve population estimates of fisheries in the CCE.

Data and Methods

Data were obtained from the CalCOFI Cast and Bottle database (https://calcofi.org/) from research cruises over the time period 1949-2019. Records of temperature, salinity, and dissolved oxygen are used for the period 1984 - 2019. An ichthyoplankton dataset collected by CalCOFI (https://calcofi.org/) was used as a proxy for spawning adult fish populations (Koslow et al., 2011; Schroeder et al., 2019). Records for eight fish species representing the southern

mesopelagic, northern mesopelagic, coastal pelagic, and benthic habitat categories in the CCE were included (Table 3.1). Due to changes in ichthyoplankton nets, the time series 1984 - 2019 was chosen for consistency of data. The four habitat categories used in this analysis spawn in the spring (March - May) and/or summer (May - September), so only records from these months were chosen.

A time series of larval abundance, temperature, salinity, and dissolved oxygen concentration was created from the CalCOFI dataset for each habitat category for the spring and summer seasons. An annual mean of temperature, salinity, and oxygen was calculated between the stations and depth ranges specified for each category. The anomaly from the mean was then calculated for each of the three environmental parameters. The larval fish abundance dataset does not include depth and was averaged annually over station distance for spring and summer seasons according to.

$$\text{Larval Fish Abundance} = \log(\text{Abundance} + 1) \qquad (1)$$

A log transform is used because the data shows significant variation in fish abundance due to exponential boom and bust cycles within the ecosystem, following (Nielsen et al., 2021).

Table 3.1 A compilation of data on eight fish species representing four major habitat categories in the CCE from information compiled from several papers. Water Mass: PSUW - Pacific Subarctic Upper Water. PEW - Pacific Equatorial Water. Spawning Season – Bim: Bimodal. Ext – Extended. Vertical Dimension: upper – mean – lower or upper – lower. (H Geoffrey Moser, 1987; Hsieh et al., 2005; Moser & Smith, 1993; Smith & Moser, 1988).

Species	Habitat	Water Mass	Spawning Season	Vertical Distribution
Stenobrachius leucopsarus	Northern Mesopelagic	PSUW	Spr/Feb-May	75-87.5-200
Tarletonbeania Crenularis	Northern Mesopelagic	PSUW	Spr-Sum/May-Jul	75-137.5-400
Triphoturus Mexicanus	Southern Mesopelagic	PEW	Sum/Aug	0-62.5-300
Vinciguerria	Southern Mesopelagic	PEW	Ext/Aug	0-62.5-125
Citharichthys	Benthic	PEW-PSUW	Bim/Aug,Feb	sea floor-549
Sebastes Jordani	Benthic	PEW-PSUW	Fall-Spr/Feb-Mar	sea floor-732
Scomber Japonicus	Coastal Pelagic	PEW-PSUW	Sum/Aug	0-100
Merluccius Productus	Coastal Pelagic	PSUW	Win-Spr/Feb-Mar	0-914

Results

The novel approach of this analysis is that environmental factors and larval fish abundances are examined within defined habitat boundaries on a CalCOFI line where a species is commonly found rather than over the entire grid, which can hide the influence of an individual water mass. We hypothesize that each habitat category has a unique set of environmental conditions that contribute to their abundance, and this is controlled by changes in source water concentration. Previously, Schroeder et al. (2019) found that source water changes of PSUW impact the larval abundance of rockfish in the CCE. Here we take a more generalized approach and test source water impacts on four major habitat categories.

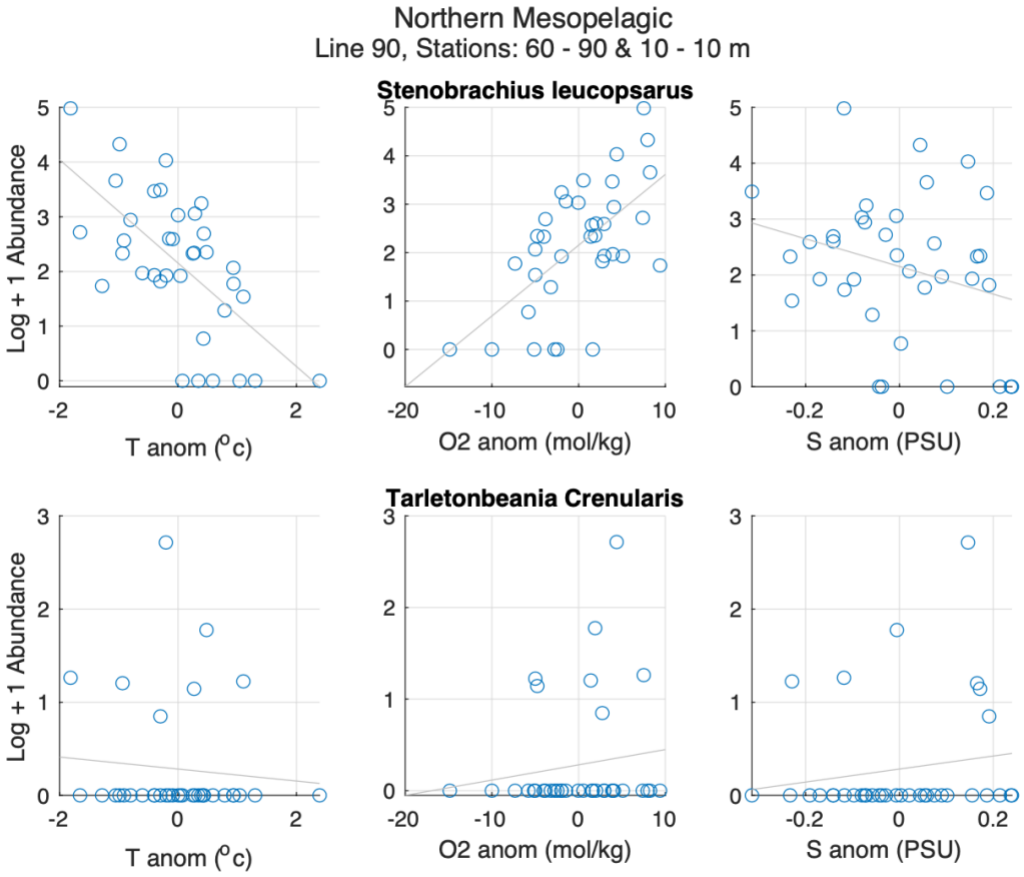

Figure 3.1 Northern mesopelagic species, Stenobrachius Leucopsarus and Tarletonbeania Crenularis from CalCOFI line 90, stations 60-90 environmental parameters measured at 10 m depth. Spring.

The northern mesopelagic habitat on line 90 is defined here as the region from 240-460 km (CalCOFI stations 60-90) offshore, which contains the two main cores of the equatorward California Current. Adult fish and larva of these two species are generally found between 75-200 meters depth (Hsieh et al., 2005), though the abundances display the strongest relationships with environmental parameters at approximately 10 meters depth. The water mass in this region is largely PSUW, characterized by low temperature, low salinity, and high oxygen concentration (Bograd et al., 2019). Though the CCE is highly dynamic and water masses are constantly

mixing from eddies and upwelling events, especially in this region, off the Southern California Bight on line 90. Figure 3.1 above, displays the relationships for the spring season measured at a depth of 10 meters. Stenobrachius Leucopsarus has a strong negative relationship with temperature, a strong positive relationship with oxygen concentration, and a very weak negative relationship with salinity. Tarletonbeania Crenularis, however, does not display any significant relationships in this region.

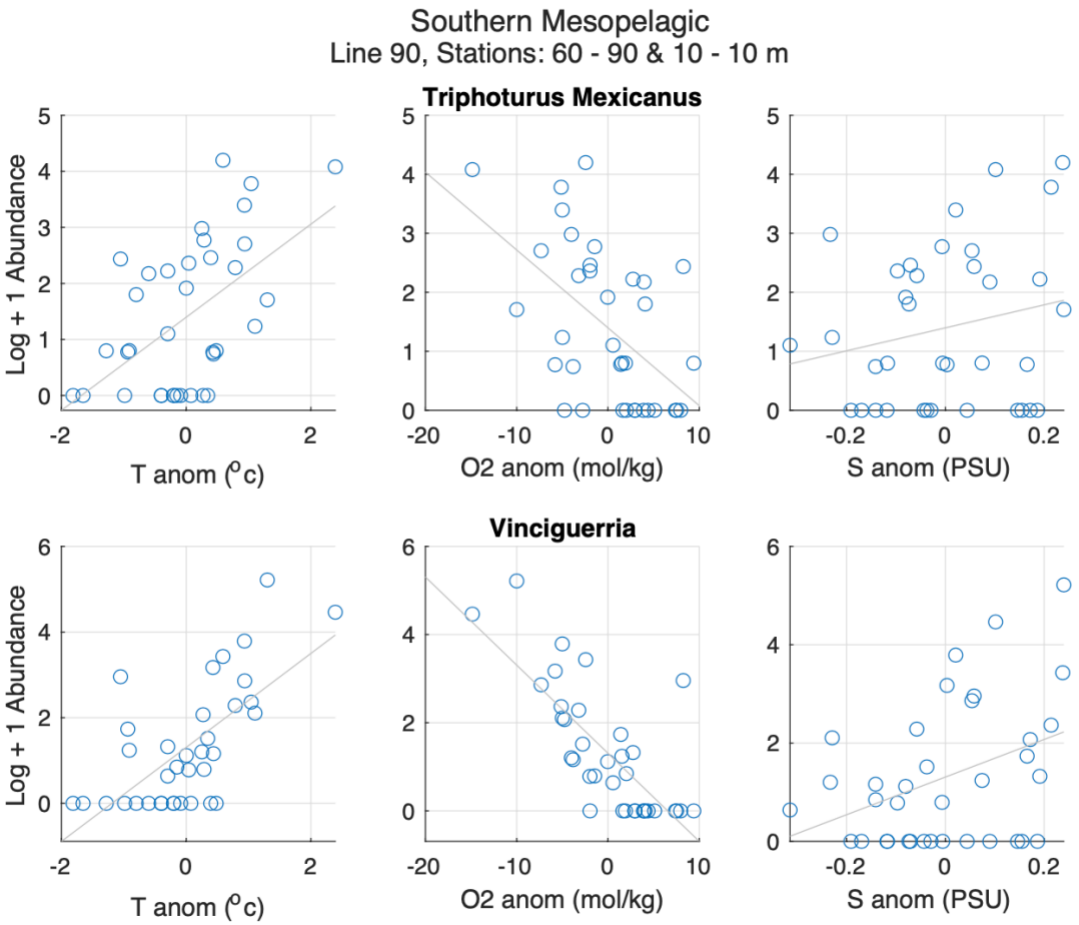

Figure 3.2 Southern mesopelagic species, Tripotorus Mexicanus and Vinciguerria from CalCOFI line 90, stations 60-90 environmental parameters measured at 10 m depth. Spring.

The spatial distribution of southern mesopelagic species has the highest concentration at the southern tip of Baja California and becomes quite sparse at Point Conception near line 80

(Ahlstrom, 1958). Prior research has associated increases in population of these species with higher SST and suggested that there has been northern range shifting of their spatial distribution as of 2015, relative to 2005 (McClatchie et al., 2016). Southern mesopelagic species are generally associated with the northward flowing PEW, or the spicy water mass characterized by high temperature, high salinity, and low oxygen concentration. This is directly reflected in figure 3.2, as both Tripotorus Mexicanus and Vinciguerria have a strong positive relationship with temperature, strong negative relationship with oxygen, and weak positive relationship with salinity. These results suggest that an increase in the concentration of the spicy water mass has a positive relationship with the abundance of southern mesopelagic species. That the relationships of southern and northern mesopelagic fish abundance with PEW and PSUW masses are so strong and opposite from one another is powerful evidence for our hypothesis that source water in a controlling factor of larval abundance.

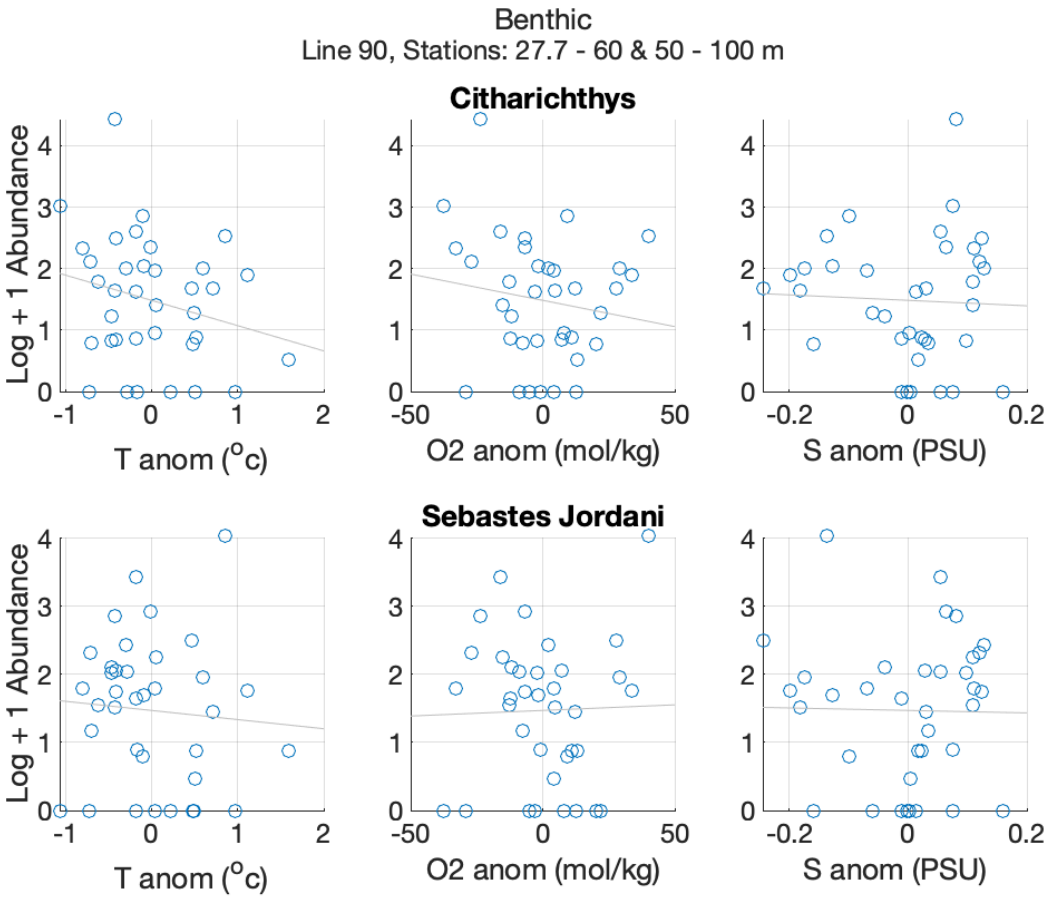

Figure 3.3 Benthic species, Citharichthys and Sebastes Jordani from CalCOFI line 90, stations 27.7-60 and environmental parameters averaged between 50-100 m depth. Spring.

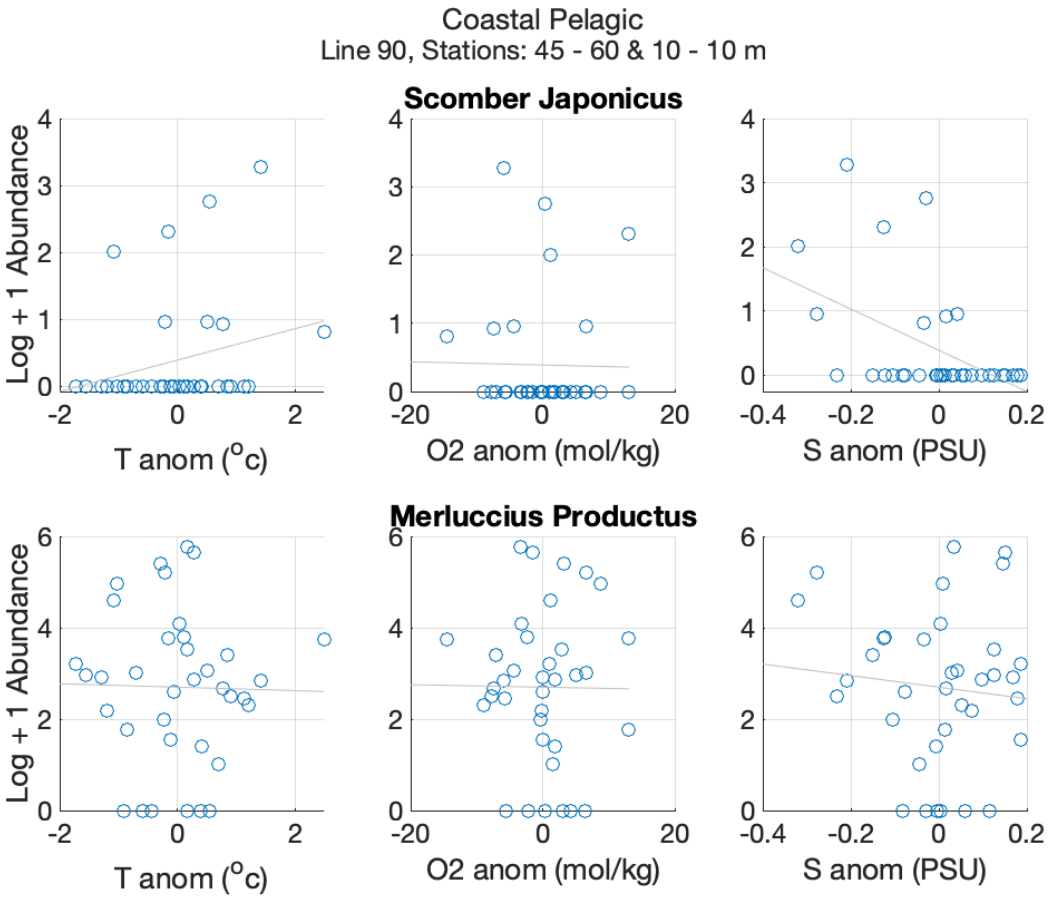

Figure 3.4 Coastal Pelagic species, Scomber Japonicus and Merluccius Productus from CalCOFI line 90, stations 45-60 and environmental parameters measured at 10 m depth. Spring.

Benthic and Coastal Pelagic species do not display any significant correlations with temperature, salinity, or oxygen concentration. However, while not significant themselves, the results highlight the importance of the strong relationships found for northern and southern mesopelagic species.

Discussion

The objective of this research is to determine whether there is a significant relationship between water mass properties and larval fish abundances of several major fisheries in the CCE. These environmental relationships, paired with accessible and high-resolution data such as CalCOFI or the CUGN, could help improve biophysical modeling research and project changes in fisheries stocks more accurately. The results show strong relationships between ichthyoplankton abundance and environmental parameters for northern and southern mesopelagic species, suggesting that source water is a controlling factor of abundance. Stenobrachius Leucopsarus abundance, a northern mesopelagic, exhibits a strong positive relationship with properties associated with the minty water mass. During periods with greater southward transport of PSUW in the California Current one would expect to see a higher abundance of these species. The second northern mesopelagic species, Tarletonbeania Crenularis, however, did not display any significant relationships, likely because the species is typically found on more northern lines, has a longer spawning season, and is an overall less abundant northern mesopelagic species than Stenobrachius Leucopsarus on these two lines. In the future, this process should be repeated on additional northern mesopelagic species that are more abundant in this region. The two southern mesopelagic species have a strong relationship with properties associated with the spicy water mass. Periods with greater transport of PEW into the region from the California Undercurrent would likely see an increase in the abundance of these species.

Another approach for this analysis could be to measure source water more directly with salinity or oxygen on an isopycnal, or constant density, surface as a biological tracer. The benefit of isopycnal surfaces over depth coordinates is that the vertical impacts of heaving are

removed, meaning that a tracer will remain largely unchanged as it advects through the CCE. This can be used to distinguish between the PSUW and PEW masses. The CUGN climatology over the period 2007-2023 on lines 66.7, 80, and 90 provides a high-resolution description of source water concentration in the CCE, and since 2017 the dissolved oxygen data, presented in the previous chapter, provides a more complete picture. This data could be used to estimate the population of major fisheries and create specialized indices that are more accurate than their basin-wide counterparts currently in use.

Previous research has found that an overall decline in dissolved oxygen concentration in the CCE has led to a decrease in larval fish abundance (Koslow et al., 2011). The results presented here suggest that although the abundance of some species, northern mesopelagics, are found to decline in periods of low oxygen concentration, other species, southern mesopelagics, are found to increase. This finding reinforces the benefit of analyzing species in their specific habitat rather than on a basin-wide scale. An implication is that the environmental factors influencing ichthyoplankton abundance are variable rather than consistent over the entire CCE.

References

Ahlstrom, E. H., and R. C. Counts. (1958). Development and distribution of Vinciguerria lucetia and related species in the eastern Pacific. *U.S. Fish. Wildl. Serv., Fish. Bull., 139*.

Bograd, S. J., Schroeder, I. D., & Jacox, M. G. (2019). A water mass history of the Southern California current system. *Geophysical Research Letters, 46*(12), 6690-6698. doi:10.1029/2019gl082685

H Geoffrey Moser, P. E. S., AND Lawrence E Eber. (1987). LARVAL FISH ASSEMBLAGES IN THE CALIFORNIA CURRENT REGION, 1954-1960, A PERIOD OF DYNAMIC ENVIRONMENTAL CHANGE. *California Cooperative Oceanic Fisheries Investigations Reports, XXVIII. 1987*.

Hsieh, C. H., Reiss, C., Watson, W., Allen, M. J., Hunter, J. R., Lea, R. N., Rosenblatt, R. H., Smith, P. E., & Sugihara, G. (2005). A comparison of long-term trends and variability in populations of larvae of exploited and unexploited fishes in the Southern California region: A community approach. *Progress in Oceanography, 67*(1-2), 160-185. doi:10.1016/j.pocean.2005.05.002

Koslow, J. A., Goericke, R., Lara-Lopez, A., & Watson, W. (2011). Impact of declining intermediate-water oxygen on deepwater fishes in the California Current. *Marine Ecology Progress Series, 436*, 207-218. doi:10.3354/meps09270

McClatchie, S., Goericke, R., Leising, A., Auth, T. D., Bjorkstedt, E., Robertson, R. R., Brodeur, R. D., Du, X. N., Daly, E. A., Morgan, C. A., Chavez, F. P., Debich, A. J., Hildebrand, J., Field, J., Sakuma, K., Jacox, M. G., Kahru, M., Kudela, R., Anderson, C., Lavaniegos, B. E., Gomez-Valdes, J., Jimenez-Rosenberg, S. P. A., McCabe, R., Melin, S. R., Ohman, M. D., Sala, L. M., Peterson, B., Fisher, J., Schroeder, I. D., Bograd, S. J., Hazen, E. L., Schneider, S. R., Golightly, R. T., Suryan, R. M., Gladics, A. J., Loredo, S., Porquez, J. M., Thompson, A. R., Weber, E. D., Watson, W., Trainer, V., Warzybok, P., Bradley, R., & Jahncke, J. (2016). State of the California Current 2015-16: Comparisons with the 1997-98 El Nino. *California Cooperative Oceanic Fisheries Investigations Reports, 57*. Retrieved from <Go to ISI>://WOS:000392962400001

Moser, H. G., & Smith, P. E. (1993). Larval Fish Assemblages and Oceanic Boundaries. *Bulletin of Marine Science, 53*(2), 283-289. Retrieved from <Go to ISI>://WOS:A1993MN60600001

Nielsen, J. M., Rogers, L. A., Brodeur, R. D., Thompson, A. R., Auth, T. D., Deary, A. L., Duffy-Anderson, J. T., Galbraith, M., Koslow, J. A., & Perry, R. I. (2021). Responses of ichthyoplankton assemblages to the recent marine heatwave and previous climate fluctuations in several Northeast Pacific marine ecosystems. *Global Change Biology, 27*(3), 506-520. doi:10.1111/gcb.15415

Rudnick, D. L., Zaba, K. D., Todd, R. E., & Davis, R. E. (2017). A climatology of the California Current System from a network of underwater gliders. *Progress in Oceanography, 154*, 64-106. doi:10.1016/j.pocean.2017.03.002

Schroeder, I. D., Santora, J. A., Bograd, S. J., Hazen, E. L., Sakuma, K. M., Moore, A. M., Edwards, C. A., Wells, B. K., & Field, J. C. (2019). Source water variability as a driver of rockfish recruitment in the California Current Ecosystem: implications for climate change and fisheries management. *Canadian Journal of Fisheries and Aquatic Sciences, 76*(6), 950-960. doi:10.1139/cjfas-2017-0480

Smith, P. E., & Moser, H. G. (1988). Calcofi Time-Series - an Overview of Fishes. *California Cooperative Oceanic Fisheries Investigations Reports, 29*, 66-78. Retrieved from <Go to ISI>://WOS:A1988U633200006

Conclusion

The overarching theme of this thesis is high resolution observations of changes in the North Pacific Ocean. The three chapters describe 1) changes in the dominant modes of North Pacific sea surface temperature including the impacts on the PDO Index, 2) an analysis of oxygen anomalies from the annual cycle in the CCE using the CUGN, and 3) the impact of source water changes on ichthyoplankton abundance.

A key takeaway from chapter one is that the first few spatial modes of SST have significantly changed as a direct result of the marine heatwaves and the PDO is no longer the best descriptor of variance in the North Pacific. In addition, we find that the second spatial mode has risen in importance and is now necessary to describe much of the warming across the Central and Western Pacific.

The results from chapter two suggest that source water advecting northward from the equator, or Pacific Equatorial Water (PEW), is a primary source of low oxygen anomalies in the California Current region. Additionally, Hovmoller diagrams reveal oxygen and salinity anomalies that tilt offshore over time and joint-pdfs of dissolved oxygen – salinity further suggest that the across-shore propagation of subthermocline eddies (STEs) is largely responsible for the offshore transport of PEW. These results confirm previous research on STEs for the anomaly data field. In the future, there is more work to be done understanding physical processes that cause the high oxygen anomalies from the annual cycle.

In chapter three, we find that an increase in Pacific Subarctic Upper Water (PSUW) is associated with higher abundance of northern mesopelagic species and that an increase in Pacific Equatorial Water is associated with an increase in southern mesopelagic species. Ultimately strong correlations between environmental factors and ichthyoplankton abundance could allow

high resolution data networks, such as CalCOFI or CUGN to estimate the adult populations of fish species.